1   # Kinetic behavior of partially dehydroxylated kaolinite

2   # Revision 1

3

4   Victor A. Drits [1]* and Arkadiusz Derkowski [2]

5   [1] Geological Institute of the Russian Academy of Science, Pyzhevsky per. 7, 119017 Moscow, Russia

6   [2] Institute of Geological Sciences, Polish Academy of Sciences, Senacka 1, 31-002 Krakow, Poland

7   * corresponding author; e-mail: victor.drits@mail.ru

8

9   **Abstract**

10   The multi-cycle heating and cooling thermogravimetric (TG) method was used to

11   study the kinetic behavior of three kaolinite samples: defect-free Keokuk kaolinite, KGa-2

12   with a very low degree of structural order, and KGa-1 having intermediate structural order. In

13   each cycle, the maximum cycle temperature (MCT) was set to 25ºC higher than the preceding

14   cycle. The TG patterns consist of a set of subsequent DTG maxima representing the portions

15   of OH groups that did not dehydroxylate in previous cycles.

16   Each stage of partial dehydroxylation consists of two kinetic mechanisms and for each

17   of them the experimental $d\alpha/dt$ values that characterize the reaction rate of the dehydroxylated

18   fraction, α, within a period of the reaction time, t, were computed. One mechanism

19   corresponds to a zero-order reaction that occurs in each cycle and indicates that the reaction is

20   homogeneous and each non-dehydoxylated layer is transformed into metakaolinite layer

21   without formation of intermediate derivatives. For this step of the cycles activation energy, E_a,

22   was calculated from the linear relationship between $Ln(d\alpha/dt)$ and reciprocal temperature, T;

23   for KGa-2 kaolinite, the E_a varies from 32.0 to 38.1 kcal/mol; in KGa-1, E_a varies from 37.1

24   to 40.4 kcal/mol, whereas in Keokuk, E_a varies from 42.7 to 47.5 kcal/mol. The particular

25   variation of the E_a is discussed in terms of structural and morphological features of the

26   samples.

27   The kinetic mechanism of the second step of reaction corresponds to the temperature

28   range higher than the first step of the same heating cycle. The second step starts from the

29   point where $\alpha = \alpha_p$ that was found to vary between 0.25 and 0.45. The acceleration of the

30   reaction rate of dehydroxylation within this interval decreases with increasing α and T, and the

31   mechanism observed for each of the studied samples is independent of its stacking order,

32   average particle size, and particle size distribution. The $f(\alpha)$ is a function of the reaction

33   mechanism in the second step and has the form:

34                                    $$f(\alpha) = (1 - \alpha)^n / (1 - n)$$

35   where n is an empirical parameter and its value was found from < 0.01 to 0.06-0.08 among

36   cycles and samples. The value of n controls the reaction rate slowing or the deviation from the

37   zero-order reaction and increases with increasing metakaolinite content. Using parameters n,

38   α, and T determined for the second step, E_a values were calculated for the second step of

39   reaction in each heating cycle. For the Keokuk kaolinite, E_a value varies from 31.6 to 37.5

40   kcal/mol, in KGa-1 E_a is 27.0 - 35.6 kcal/mol, and in KGa-2 the E_a value varies from 26.3 to

41   34.9 kcal/mol. A structural model explaining the acceleration rate slowing is discussed.

42

43   **Keywords**: kaolinite, dehydroxylation, reaction kinetics, thermogravimetry, stacking order

44

45

2

46   **Introduction**

47

48   **Kaolinite structure**

49   Kaolinite, $Al_4Si_4O_{10}(OH)_8$, is a common dioctahedral 1:1 layer mineral, forming large

50   and economically valuable deposits. An individual kaolinite layer consists of one alumina

51   octahedral sheet and one silica tetrahedral sheet that are bound to each other via apical oxygen

52   atoms. Strong cohesion of the adjacent layers is formed by hydrogen bonding from OH groups

53   on the basal surface of one layer to oxygen atoms forming a basal surface of the following

54   layer. Three symmetrically independent basal OH groups are referred to as "external" OH

55   groups because they form the outer basal surface of each layer. The fourth (OH) group is

56   referred to as "internal" because it is located within the layer. The octahedral sheet of the

57   kaolinite layer contains three symmetrically independent sites differing in the arrangement of

58   OH groups and oxygen atoms coordinating to two octahedral Al cations and one vacant

59   octahedron (Brindley and Robinson 1946).

60   The kaolinite layer has a fixed chemical composition, with well-determined positions

61   of each atom. However, the pattern of stacking of adjacent layers produces a large variation of

62   the kaolinite structure (Brindley et al. 1986; Bailey 1988). According to a model of Bookin et

63   al.(1989), two layers displacement vectors, t_1 and t_2, related by a pseudomirror plane passing

64   through the kaolinite layer unit cell (Bailey 1988) form defect-free enantiomorphic kaolinite

65   structures which cannot to be distinguished by XRD. A random interstratification of these

66   vectors creates stacking faults which produce most of the structural disorder of kaolinite. The

67   pattern and proportion of stacking faults have been modeled, recognized by X-ray diffraction

68   (XRD), and confirmed by high-resolution transmission electron microscopy (HRTEM;

69   Plançon et al. 1989; Kogure and Inoue 2005; Kogure et al. 2010). According to Plançon et

70   al.(1989), the Hinckley index (H.I.) can be used as a measure of stacking faults in a kaolinite

71   sample only if HI < 0.43. For kaolinite having H.I.> 0.43 , it is a measure of the relative

3

72   amount of essentially defect-free crystallites coexisting with crystallites containing larger

73   amount of stacking faults (physical mixture).

74

75   **Dehydroxylation of kaolinite**

76   The ceramic industry, either in the past or today, has stimulated intense studies on

77   kaolinite dehydroxylation. An endothermic dehydroxylation of kaolinite and the formation of

78   metakaolinite occurs in the temperature interval from 400° to 650°C. Metakaolinite is

79   considered as a semi-amorphous or amorphous immediate product of kaolinite

80   dehydroxylation (Brindley and Nakahira 1957; Yeskis et al. 1985). Metakaolinite was found

81   to contain up to 1.7 wt.% of H_2O equivalent that occurs as residual OH groups (MacKenzie et

82   al. 1985; White et al. 2013). Upon prolonged heating, metakaolinite probably progressively

83   releases H_2O (White et al. 2013). Therefore, the reaction of dehydroxylation, accompanied by

84   the transformation of kaolinite into metakaolinite is described as:

85    $Al_4Si_4O_{10}(OH)_8 \rightarrow Al_4Si_4O_{14-m} (OH)_{2m} + (4-m)H_2O\uparrow$

86   where m is up to ≈ 0.5

87   Despite decades of studies devoted to the kaolinite dehydroxylation, there is no general

88   agreement concerning the rate-controlling mechanism of this reaction, neither there is

89   consistent determination of activation energy associated with dehydroxylation. Variability in

90   the apparent activation energy and the rate-controlling mechanism obtained for kaolinite

91   dehydroxylation by different techniques is dependent on structural order-disorder, particles

92   size and their distribution, experimental conditions, presence of water vapor pressure,

93   impurities, etc. (Ortega et al. 2010; Ptáček et al. 2011, for review and references).

94   The lack of consensus for a kinetic model of kaolinite dehydroxylation is analogous to

95   the disagreement over the dehydroxylation reactions of dioctahedral 2:1 clay minerals

96   (reviewed by Drits et al. 2012a). Instead of investigating the overall kinetics of

97   dehydroxylation, continuously from the beginning to the end of a single reaction, Drits et al.

4

98   (2011b, 2012a,b) studied the kinetics of dehydroxylation of dioctahedral 2:1 layer minerals at

99   different stages of dehydroxylation. For these minerals, partial dehydroxylation follows to the

100   kinetics of zero order. Thus, the reaction is homogeneous, the rate of the reaction is not

101   dependent on the concentration of the reacted material, and the structural transformation

102   occurs without a formation of any intermediate phase.

103   Following the methodology applied to dioctahedral 2:1 layer minerals (Drits et al.

104   2012a), the multi-cycle heating and cooling technique and subsequent computation of kinetic

105   parameters has potential to determine the reaction kinetics of partial dehydroxylation of

106   kaolinite. Application of the multi-cycle heating-cooling TG analysis (Slonimskaya et al.

107   1972; Drits and McCarty 2007; Drits et al. 2011b, 2012a; Derkowski et al. 2012) revealed

108   numerous advantages: (1) analysis allows the tracking of mass evolution of the sample

109   continuously at different stages of dehydroxylation after step-heating and subsequent

110   stabilization of the sample during the cooling stage, (2) analysis prevents complications from

111   sample to sample or portion to portion heterogeneity, thus the mass loss and gain between the

112   cycles can be calculated precisely, (3) analysis prevents complications coming from the

113   variability of water vapor content at different stages of partial dehydroxylation (Drits et al.

114   2011b, 2012a), and (4) partial dehydroxylation using heating-cooling is analogous to majority

115   of *ex-situ* measurements (by nuclear magnetic resonance, XRD, infrared spectroscopy) often

116   performed on pre-heated, partially dehydroxylated samples.

117   Describing thermal behavior and kinetics of partially dehydroxylated kaolinite, as a

118   function of the particle size distribution, the degree of structural order, and the influence of the

119   new-formed metakaolinite, is the main purpose of the present study.

120

5

121   **Samples**

122   **Structural features**

123   Clay Minerals Society' source clay kaolinite KGa-1 and KGa-2, and the Keokuk

124   kaolinite (Bish and von Dreele 1989; Bish 1993) were used in the study.

125   Powder X-ray diffractometry (XRD) was used to analyze bulk samples and two coarse

126   size fractions (> 4 μm and 1-4 μm) in a randomized mode ensuring no preferred orientation of

127   crystallites by applying a side-loading XRD holder. The X'TRA XRD (Thermo) was

128   equipped with a solid state SiLi point detector with an electronic energy discrimination

129   window. CuKα radiation was used to record the randomized powder within 5-65 º2Θ range,

130   with a step of 0.01 º2Θ, and irradiation time of 10 sec/step.

131   The XRD pattern of the Keokuk kaolinite contains very sharp, intense and well

132   resolved *hkl* reflections owing to its defect-free, triclinic, one-layer structure (Bish and Von

133   Dreele 1989; Bish 1993). The structure of KGa-2 kaolinite contains high structural disorder

134   related to a random interstratification of the two layer stacking displacement vectors. As a

135   result, the diagnostic 11*l* and 02*l* XRD reflections are weak or absent. The KGa-1 kaolinite

136   contains stacking faults observed in the diagnostic 11*l* and 0*2l* XRD reflections that are

137   significantly weaker, wider and less-resolved compared to the XRD pattern of the Keokuk

138   sample (Fig. 1). Both the KGa-1 and KGa-2 samples were separated by centrifugation in a

139   water suspension into three grain size fractions: >4 μm, 4-1 μm, and < 1 μm, respectively. In

140   KGa-1 and KGa-2, the two coarse fractions prevail by mass and the fraction < 1 μm yielded

141   only minor amounts. For the XRD patterns of KGa-1, the stacking order in the fraction of 4-1

142   μm is greater than that in the coarser, > 4 μm fraction, (Fig. 1b). However, the full width at

143   half height (FWHH) of 00*l* reflections of the fraction of > 4 μm is slightly narrower than those

144   corresponding to the fraction of 4-1 μm of the KGa-1 sample (Fig. 1b). Thus, the average

145   thickness of the crystallites comprising the fraction of > 4 μm is slightly larger than that is the

146   fraction of 4-1 μm.

6

147

Particle size distribution (PSD)

149   The PSD of bulk samples was determined using a Microtrac S3000 laser particle-size

150   analyzer. Approximately 30 mg of sample was sonicated for 30 seconds in isopropyl alcohol

151   to avoid clay swelling, and laser scanned three times for 30 seconds each. The presented data

152   is an average of the three scans.

153   The KGa-1 sample shows a bimodal PSD with maxima located at 3 μm and 22 μm

154   (Fig. 2). The PSD shape of KGa-2 sample is unimodal with mean size < 11 μm, and with little

155   asymmetry towards finer particles. The Keokuk sample analyzed for PSD shows the average

156   particle size close to 10 μm (Fig. 2). Because of a sharp and narrow pattern of PSD shape of

157   Keokuk kaolinite, all its particles remain > 4 μm size, therefore, no yield was produced by

158   separating any finer fraction.

159

160

161   **Methods**

162   Thermogravimetic (TG) experiments at a constant heating rate of 2°C/min or 5°C/min,

163   from 25 to 1000°C, are referred hereafter as TG screen analyses. The TG screen was

164   performed to identify the temperature range of dehydroxylation, to determine the shape of the

165   DTG (1st derivative of TG) peak, and to find the temperature of maximum rate of

166   dehydroxylation. The TA Discovery IR model thermal analyzer with a weighing error of < 1

167   μg, weight measurement resolution of < 0.1 μg, and a thermal drift between 200 and 1000°C

168   of < 4 μg was used in the TG screen analysis, with 20 mg of a sample. In addition to the bulk

169   sample analysis, a TG screen was performed for each of the three separated grain size

170   fractions of KGa-1 and KGa-2 samples. To determine the evolution of H_2O molecules at

171   different stages of the kaolinite dehydroxylation, the multi-cycle heating and cooling TGA

172   method of Slonimskaya et al. (1972) modified by Drits and McCarty (2007), Derkowski et al.

7

173   (2012), and Drits et al. (2011b, 2012a) was applied. The analysis was a set of consecutive

174   heating cycles separated by intervals of rapid cooling with the maximum heating temperature

175   of a cycle incrementally higher than the preceding cycle. The thermal conditions of the OH-

176   H_2O evolution in the heating-cooling method are significantly different from the TG screen

177   analysis.

178   The heating-cooling analysis was performed using the same TG instrument as in the

179   TG screen analysis, and 20 mg of sample. The heating rate for all cycles was fixed at

180   2.5^{o}C/min, and the sample chamber was constantly purged during analysis with 5.0N purity

181   nitrogen gas at a flow rate of 50 ml/min. The maximum cycle temperature (MCT) of the first

182   cycle was 250°C, for the next two heating cycles the MCT was 50°C higher than the

183   maximum temperature of the preceding cycle. The maximum temperature increment was

184   decreased to 25°C for the following 7-13 cycles corresponding to the dehydroxylation range.

185   After MCT was reached, the cooling stage started and the temperature dropped to 100°C

186   before initiation of the next heating cycle. Because infrared heating is used in the TA

187   Discovery IR device, cooling from MCT to 100°C was rapid, within < 60 sec., under

188   continuous gas purge as above, to avoid rehydroxylation effects (Derkowski et al. 2012).

189

190

191   **Kinetic analysis**

192   The kinetics of solid-state reactions, describing the reaction rate $d\alpha/dt$ can be

193   expressed by the general kinetic equation

194   $$\frac{d\alpha}{dt} = Ae^{\frac{-E_a}{RT}} f(\alpha) \qquad (1)$$

195   where α is the fraction of the sample reacted within a period of the reaction time, t, and $f(\alpha)$ is

196   a function of the reaction mechanism; T is the absolute temperature (^{o}K), R is the gas constant,

197   A is the pre-exponential factor of the Arrhenius equation, and E_a is the activation energy.

8

198   In its logarithmic form, Equation 1 is:

199
$$Ln \frac{d\alpha/dt}{f(\alpha)} = Ln(A) - \frac{E_a}{RT}$$
(2)

200   When the $f(\alpha)$ function is determined accurately, a plot of the left side of Equation 2

201   versus $1000/T$ is a straight line. The activation energy is determined from the slope of the line

202   and the pre-exponential factor is represented by its intercept.

203   The $f(\alpha)$ functions proposed for solid-state reactions depend on simplified physical

204   models, although many experiments show a deviation from such models. Perez-Maqueda et

205   al. (2006) suggested that deviations from the ideal models imply a limitation to the kinetic

206   analysis because none of the $f(\alpha)$ equations proposed can properly fit all the experimental

207   data. Perez-Maqueda et al. (2006) showed that a modification of the empirical Sestak-

208   Berggren equation (Sestak and Berggren 1971) in the form:

209
$$f(\alpha) = c(1-\alpha)^n \alpha^m$$
(3)

210   can describe equally well the equations corresponding to ideal models for solid-state

211   reactions if c, n and m parameters are determined correctly. Based on the set of different

212   reaction models given in Table 3 of Vyazovkin et al. (2011), the common function of c can be

213   written as

214
$$c = (1-n)^{-1}(1-m)^{-1}$$
(4)

215   The modified Sestak-Berggren equation of the $f(\alpha)$ function can be successfully

216   applied for kinetic analysis of the experimental data without any preliminary assumption

217   about the kinetic model (Perez-Maqueda et al. 2006). Combining equations 2 and 3, the

218   experimentally applicable equation is:

219
$$Ln \frac{d\alpha/dt}{(1-\alpha)^n \alpha^m} = Ln(cA) - \frac{E_a}{RT}$$
(5)

220   Using the gradient, non-smooth optimization model with the Solver® program (Nenov

221   and Fylstra 2003), for each heating cycle showing a significant portion of dehydroxylation,

9

222   the best linear correlation between the left side of the Equation 5 and $1000/T$ was found by

223   fitting the n and m parameters. Thus, the E_a can be obtained from the slope of the linear trend

224   line (Drits et al. 2011b, 2012b).

225

226

227   **Results**

228   **TG screen patterns.**

229   TG screen of the Keokuk sample revealed two sharp DTG peaks, at 641° and 663^oC,

230   and a broad DTG maximum at about 598^oC. These maxima temperatures are significantly

231   higher than those observed for KGa-1 and KGa-2 which are equal to 479 and 460^oC,

232   respectively. The DTG curve of KGa-1 contains a high-temperature shoulder with an apparent

233   maximum at 569^oC (Fig. 3a). The separated size fractions from the KGa-2 sample show

234   similar DTG peak shapes, FWHH, and similar maximum dehydroxylation temperatures (Fig.

235   3b), suggesting that the particles of different size formed by aggregation of small crystallites

236   of similar structure and texture.

237   The temperature of maximum DTG peak in the > 4 μm fraction of KGa-1 is 534^oC

238   which is significantly higher than those temperatures corresponding to the finer fractions: 513

239   ºC and 509 ºC, for the 1-4 μm and < 1 μm, respectively. The > 4 μm fraction of KGa-1 has a

240   high temperature shoulder with an apparent DTG maximum ~ 644 ºC (Fig.3b). The significant

241   difference of the temperature of maximum dehydroxylation between the grain size fractions of

242   KGa-1 (Fig. 3b) corresponds to its bimodal PSD (Fig. 2). The coarser fraction (> 4 μm) with

243   the highest temperature of maximum dehydroxylation has, however, a lower degree of

244   structural order than the finer fraction (1-4 μm; compare Fig. 1b and Fig. 3b).

245

246

247   **Heating-cooling experiments.**

248   In general, the mass loss effects observed for the studied samples subjected to

249   subsequent heating-cooling cycles are similar (Fig. 4). Each heating interval consists of a

250   single strong high-temperature DTG maximum. This DTG maximum resulting from the

251   dehydroxylation of the previously not dehydroxylated OH groups begins at a point where the

252   mass is lower than the lowest mass from previous cycles (M_S). The reaction is complete at the

253   MCT or during the initial portion of the following cooling stage where the temperature is

254   sufficiently high to maintain the dehydroxylation reaction owing to thermal inertia and heat

255   capacity (M_e) (Fig. 5a). Thus, the high-temperature DTG peak represents the portion of the

256   sample that did not dehydroxylate in previous cycles. Noticeable, no middle-temperature DTG

257   peak has been observed (Derkowski et al. 2012).

258   The DTG peaks were used to analyze the main features of mass evolution during

259   heating and cooling cycles. In KGa-1 and KGa-2, the evolution of the intensity of the high-

260   temperature DTG maxima along the heating-cooling cycles form a bell-like shape over

261   increasing MCT (Fig. 4). In contrast, the DTG peaks of the Keokuk sample shows, despite

262   small fluctuations, that the intensities continuously increase with an increasing MCT (Fig.4).

263   To quantify the mass loss with temperature, a degree of dehydroxylation, D_T, was determined

264   after each cycle. The D_T value was calculated using the mass losses corresponding to the high-

265   temperature DTG peak ($M_S - M_e$) normalized to the dehydroxylated mass of a sample for all

266   cycles from C_o corresponding to the beginning of dehydroxylation to the particular

267   dehydroxylation cycle, C_x. The result was normalized to the total mass loss range ($M_S - M_e$)

268   for all cycles where dehydroxylation is observed (from C_o to the final cycle of

269   dehydroxylation, C_f).

270
$$D_T = \frac{\sum_{C_0}^{C_X}(M_S - M_X)}{\sum_{C_0}^{C_f}(M_S - M_e)} \times 100 \qquad (6)$$

11

271   Mass evolution of each sample can be characterized quantitatively using the

272   relationships between the D_T and the corresponding MCT. The observed dehydroxylation

273   (from 0 to 100%) of the studied samples occurs at different temperature ranges: from 375 to

274   525°C in KGa-2, from 400 to 600°C in KGa-1, and from 425 to 675°C in Keokuk kaolinite

275   (Table 1). Whereas in the KGa-2 sample, only three subsequent cycles with MCT at 425, 450,

276   and 475°C are sufficient to change the D_T from 21.3 to 80%, in Keokuk five cycles, within

277   525-625°C, are required to cover nearly the same range of D_T increase (Table 1).

278

279

280   **Calculation of kinetic parameters**

281   **Application of Equation 5 to the experimental data**

282   Dehydroxylation of clay minerals is a thermally activated reaction; determining the

283   kinetic parameters of the reaction is critical to understand the rate-controlling mechanism of

284   the process at each stage of partial dehydroxylation. In the heating-cooling technique, the

285   high-temperature DTG peak represents the portion of the sample that had not dehydroxylated

286   in previous cycles and the dehydroxylation of the original OH groups from the unaltered

287   portion at each given cycle is independent of the dehydroxylation reaction that occurs in the

288   previous cycles. Under these conditions, the dynamic DTG data and conversional equations

289   can be applied to the kinetic study of a sample separately after each heating cycle (Drits et al.

290   2011b, 2012a).

291   The calculations of kinetic parameters describing the reaction in a given cycle begins

292   at the M_S point. The final mass corresponds to M_f, the point where the slope of the DTG curve

293   significantly changes and the rate of acceleration of dehydroxylation decreases, as observed

294   from the 1st derivative of DTG (Fig.5b). Therefore, $\alpha = (M_s - M)/(M_s - M_f)$, where M is the

295   sample mass at time *t*. For the high-temperature DTG maximum of each heating interval the

296   experimental $d\alpha/dt$ values were calculated. Each $d\alpha/dt$ is equal to the change of α after

12

297   heating during 7 second increments. The analysis of the relationships between $Ln(d\alpha/dt)$

298   versus $1000/T$ plotted for each heating interval has shown that, in general, partial

299   dehydroxylation consists of two kinetic reactions (Fig.6). One reaction is represented by a

300   straight line (Figure 6) and corresponds to the zero-order kinetics occurring within a specific

301   interval of the reaction where α varies from 0 to α_p. The function $f(\alpha) = 1$ ($n = m = 0$) and

302   thus Equation 2 is rewritten as follows

303    $$Ln\frac{d\alpha}{dt} = Ln(A) - \frac{E_a}{RT} \qquad\qquad (7)$$

304   Therefore, for $\alpha \leq \alpha_p$, the activation energies can be determined directly from the slope of the

305   straight lines of $Ln(d\alpha/dt)$ over $1000/T$.

306   In each heating cycle, α_p and the corresponding temperature T_P values separate two

307   reactions with a unique $f(\alpha)$. Two relationships between the experimental $Ln(d\alpha/dt)$ versus

308    $1000/T$ and between the $Ln(d\alpha/dt)$ versus α are superimposed in the plot on Fig. 7. One

309   relationship is used to determine the point $Ln(d\alpha/dt)_p$ where $d\alpha/dt$ over $1000/T$ trend line

310   deviates from the straight line corresponding to the reaction with $f(\alpha) = 1$; this inflection point

311   indicates the rate of reaction starts to decrease. The line parallel to the abscissa and passing

312   the $Ln(d\alpha/dt)_p$ point crosses the curve of the $Ln(d\alpha/dt)$ versus α at the α_p point (Figs. 6 and 7).

313   The second mechanism corresponds to the second step of the same heating stage and begins

314   from α_p and T_p and ends at $\alpha = 1$, at the temperature T_f.

315   To determine the mechanism for the decreasing acceleration of dehydroxylation

316   reaction at the step of $\alpha > \alpha_p$, and $T > T_p$, the values of n and m parameters in the $f(\alpha)$,

317   corresponding to the linear fit between the left side of Equation 5 versus $1000/T$, were

318   obtained. The optimization procedure applied to $d\alpha/dt$ has shown that optimization occurs

319   where $m = 0$ and n values varied from cycle to cycle in each sample and from sample to

320   sample within 0.008-0.078 (Table 1). As presented above, if $m = 0$, then $c = 1/(1 - n)$ and

321   Equation 5 is rewritten as:

13

322
$$Ln\frac{d\alpha/dt}{(1-\alpha)^n} = Ln(A) - Ln(1-n) - \frac{E_a}{RT} \qquad (8)$$

323   The activation energies can be calculated for each second step of a given heating

324   interval. Equation 8 is thus rewritten:

325
$$Ln\left(\frac{d\alpha}{dt}\right)_\alpha = Ln\frac{(1-\alpha)^n}{1-n} + Ln\left(Ae^{\frac{-E_a}{RT}}\right) = Ln[f(\alpha)] + Ln[f(T)] \qquad (9)$$

326   Under non-isothermal conditions, both $f(\alpha)$ and $f(T)$ functions vary simultaneously.

327   For $\alpha_p < \alpha < 1$, $Ln(f(T))$ has a linear dependence on the reciprocal temperature whereas

328   $Ln(f(\alpha))$ depends on α, T, and n. For each $n < 1$, an increase of α occurs with an increase of

329   $|Ln(f(\alpha))|$, thus the higher n the higher $|Ln(f(\alpha))|$. In contrast, the higher α, the smaller $1000/T$.

330   Therefore, the relationship between $Ln(f(\alpha))$ and $1000/T$ at each n represents a curve where

331   the $Ln[(1-\alpha)^n/(1-n)]$ values increase with decreasing $1000/T$ (Fig. 8). A sum of the $Ln(f(\alpha))$

332   and $Ln(f(T))$ reproduces the second step of the experimental relationship of $Ln(d\alpha/dt)$ *versus*

333   $1000/T$.

334   If the correlation coefficient, r^2, of the kinetic model is < 0.95, the parameter is not

335   considered in the interpretation. The $r^2 < 0.95$ occurs in a last cycle of Keokuk and KGa-1

336   samples, where the new portion of dehydroxylated sample is very low.

337   To present the degree of dehydroxylation separately in subsequent steps of $\alpha < \alpha_p$, and

338   $\alpha > \alpha_p$, the mass loss was computed separately in each step of each cycle ($M_S - M_P$ and $M_P -$

339   M_f, respectively) and normalized to the total mass loss within these steps for all cycles where

340   dehydroxylation was observed, in a similar manner as in the Equation 1. Therefore,

341
$$DT_1 = \frac{\displaystyle\sum_{C_0}^{C_X}(M_S - M_P)}{\displaystyle\sum_{C_0}^{C_f}(M_S - M_f)} \times 100 \qquad \text{Eq. (10a)}$$

and

14

342
$$DT_2 = \frac{\sum\limits_{C_0}^{C_X}\left(M_P - M_f\right)}{\sum\limits_{C_0}^{C_f}\left(M_S - M_f\right)} \times 100$$
                              Eq. (10b)

343   Where DT_1 and DT_2 represent the relative degree of dehydroxylation for the first ($\alpha <$

344   α_p) and the second ($\alpha > \alpha_p$) steps of the dehydroxylation reaction, respectively (Table 1). The

345   T_p and T_f points are high-temperature boundaries for the DT_1 and DT_2 intervals in each cycle,

346   therefore, they serve as reference points for the DT_1 and DT_2 evolution, respectively (Fig. 9).

347   Each sample shows a range of T_p and T_f where the most significant portion of partial

348   dehydroxylation occurs (Table 1; Fig. 9). Qualitatively, the combined shape of DT_1 and DT_2

349   distribution over T_p and T_f is similar to that of the variation of mass observed in the TG screen

350   patterns (compare Fig. 9 to Fig 3).

351

352   **Calculation for the first step of the partial dehydroxylation; $f(\alpha) = 1$**

353   The E_a calculated for $\alpha < \alpha_p$ for each cycle of a sample, using Equation 7 reach

354   different maximum values and vary with partial dehydroxylation DT_1 and T_P (Table 1;

355   Fig.10). In KGa-2, E_a increases at the beginning of the reaction from 32.2 kcal/mol at $DT_1 =$

356   4.6% and $T_P = 382^{o}C$ to its maximum values of $38.1 - 38.2$ kcal/mol at $DT_1 = 23.7 - 35.7\%$

357   and $T_P = 425 - 437^{o}C$, and then decreases to 33.5 kcal/mol at $DT_1 = 41.5\%$ and $T_P = 478^{o}C$

358   (Table 1, Fig.10). In KGa-1, for the first two heating cycles the E_a increases from 25.9

359   kcal/mol at $DT_1 = 1.8\%$ and $T_P = 377^{o}C$ to 36.8 kcal/mol at $DT_1 = 4.7\%$ and $T_P = 406^{o}C$.

360   Except for these two cycles, the E_a of partial dehydroxylation in KGa-1 is almost independent

361   of DT_1 and T_P values, varying within a very narrow range, from 39.3 to 40.8 kcal/mol (Table

362   1, Fig.10). In contrast to the KGa-1 and KGa-2, the Keokuk kaolinite E_a slightly decreases at

363   the beginning of reaction from 44.1 kcal/mol at $DT_1 = 1.0\%$ and $T_P = 429^{o}C$ to its minimum

364   value of 43.2 kcal/mol at $DT_1 = 9.4\%$ and $T_P = 499^{o}C$ and then increases to 47.9 kcal/mol in

365   the heating cycle at $DT_1 = 25.4\%$ and $T_P = 577\ ^{o}C$.

15

366   A common feature of the samples is that the T_P becomes higher along with the

367   increase of MCT and D_T (Table 1). The T_P value of the first cycle, where DT_1 was sufficiently

368   high to use it for determination of the kinetic parameters, shows the values of 382, 406, and

369   429°C, corresponding to the order of KGa-2 → KGa-1 → Keokuk (Table 1).

370

371   **Calculation for the second step of the partial dehydroxylation; $f(\alpha) = (1 - \alpha)^n/(1 – n)$**

372   The E_a of the second step ($\alpha > \alpha_p$) calculated by Equation 8 is significantly lower than

373   E_a of the first step ($\alpha < \alpha_p$) for the same heating cycle. This relationship is observed for all

374   cycles in the samples (Table 1), although each sample has a different E_a distribution over DT_2

375   and T_f (Fig.10). In the KGa-2, the E_a values increase at the beginning of the reaction from

376   31.2 kcal/mol at $DT_2 = 5.8\%$ and $T_f = 399^o$C to 34.9 kcal/mol at $DT_2 = 13.6\%$ and $T_f = 424^o$C

377   and then E_a decreases to 26.3 kcal/mol at $DT_2 = 58.5\%$ and $T_f = 505^o$C (Table 1, Fig.10).

378   Similarly, in KGa-1, within the temperature interval of T_f from $424\,^o$C to $493\,^o$C the E_a values

379   increase at the beginning of the reaction from 35.6 kcal/mol at $DT_2 = 5.8\%$ to the maximum

380   value at 37.5 kcal/mol at $DT_2 = 14.2\%$ and then E_a decreases down to 27.0 kcal/mol at $DT_2 =$

381   56.8%. However, at higher T_f, the E_a values in KGa-1 increase slightly (Table 1, Fig.11).

382   The activation energy for the Keokuk sample decreases from 37.5 kcal/mol at the

383   beginning of the reaction to its minimum of 31.6 kcal/mol at $DT_2 = 15.5\%$ and $T_f = 524^o$C and

384   then increases to 36.2 kcal/mol at $DT_2 = 57.3\%$ and $T_f = 624^o$C (Fig.10). For the last two

385   cycles, the DTG curve, as T_f (Figure 4) is approached and $Ln(d\alpha/dt)$ over 1000/T plots near

386    $\alpha=1$ (Figure 6), differs from the pattern as other cycles at $\alpha > \alpha_p$. This result suggests that an

387   additional reaction contributes to the curve by disturbing the mass loss in that range. Because

388   these two last cycles are at high temperatures of $T_f = 649\,^o$C and $659\,^o$C which is typical for

389   decarbonization, the decomposition of trace carbonates is probably a factor. The kinetic

390   parameters were thus not calculated for dehydroxylation occurring at $\alpha > \alpha_p$ for the two last

391   cycles of Keokuk.

16

392   In all samples, the value of n progressively increases with an increase of DT_2 and

393   MCT from < 0.01 to 0.058 – 0.076 (Table 1, Fig.11). The T_f and MCT values coincide for all

394   cycles in Keokuk kaolinite, but the T_f values of the last two cycles in KGa-2 and last three

395   cycles in KGa-1 samples are lower by $10 – 30^oC$ then the corresponding MCT (Table 1).

396

397

398   **Discussion.**

399   **Factors controlling dehydroxylation of kaolinite**

400   In the layer stacking sequence in the defect-free kaolinite structure, referred as to

401   kaolinite $1A$, the troughs and ridges of the corrugated OH surface are parallel to the [100]

402   direction and mesh with similar corrugations of the basal oxygen atoms across the interlayer

403   (Bish and Von Dreele 1989). The O···H vectors of the three symmetrically independent

404   surface OH groups are quasinormal to the (001) to form hydrogen bonds to the adjacent layer

405   in the structure (Bish 1993). This arrangement creates a strong attraction between adjacent 1:1

406   layers. In contrast, a stacking disorder disturbs this arrangement of the hydrogen bonds as

407   described for the 1A polytype, decreasing the cohesion of 1:1 layers. Therefore, stacking

408   order-disorder is probably a factor that controls the stability of kaolinite layers during

409   dehydroxylation (Dubois et al. 1995; Franco et al. 2003, 2004; Ptáček et al. 2013). As

410   observed in the samples studied, the higher structural disorder in kaolinite (KGa-2 > KGa-1 >

411   Keokuk), the lower temperature is required for its dehydroxylation (460, 479, and 598-663ºC,

412   respectively; Fig. 3a).

413   The maximum thickness of a kaolinite1:1 layer is 4.343Å whereas the d(001) value is

414   7.156Å (Bish and Von Dreele 1989). The thickness of the interlayer space is 2.817Å whereas

415   the effective diameter of the H_2O molecule is ≈ 3.0Å. Significant energy is thus required to

416   increase the interlayer to allow H_2O molecules formed during dehydroxylation within the

417   octahedral sheet to migrate out of the structure. Rapid dehydroxylation of all OH groups

17

418   within a 1:1 layer results a high concentration of H_2O molecules which creates water vapor

419   pressure. At sufficient temperatures, the water vapor pressure can overcome the attraction of

420   adjacent layers. An increase of temperature increases the thermal vibrations of atoms,

421   increasing the unit cell volume and weakening bonds.

422   It is usually assumed that a population of larger particles separated from the bulk

423   sample would consist of larger crystallites compared to the average crystallite size found in

424   finer particles. The term of "larger" versus "smaller" crystallites should also refer to a certain

425   unit cell dimension, where crystallite thickness may or may not be related to the (*ab*) plane

426   dimension of a crystallite. Crystallites of the same or similar (*ab*) plane size or thicknesses

427   along *c** direction are aggregated in particles of different grain sizes, as in the case of KGa-2.

428   In contrast, bulk KGa-1 has intermediate degree of stacking order (H.I. = 1.5), and it consists

429   of two populations: one formed by defect-free crystallites and the other that is much richer in

430   defects (Fig. 1b; Plançon et al. 1989). Heterogeneity of particle and crystallite size is also

431   responsible for a broad interval of dehydroxylation temperature and for a distribution of

432   activation energies of dehydroxylation in samples subjected to the heating-cooling treatments,

433   as it occurs in 2:1 layer minerals (Drits et al. 2012a). The stacking order, crystallite size along

434   c* direction, and the (*ab*) plane size are usually interrelated. Therefore, in general, the smaller

435   the crystallite thickness, the higher their structural disorder, and the lower the temperature of

436   dehydroxylation, i.e., Keokuk > KGa-1 > KGa-2.

437   For thick crystallites of small surface area compared to volume, H_2O molecules

438   formed during dehydroxylation cannot be released quickly owing to the large mass of the

439   crystallite. In contrast, for fine particles, where the surface area is (in units) similar or greater

440   than the volume, the rate of dehydroxylation is higher because of the lower energy required to

441   open the interlayer. Therefore, the combination of a slow heating rate and thin crystallites is

442   an optimum condition to decrease the starting temperature of dehydroxylation, resulting in

443   lower activation energy at the beginning of the reaction. At $D_T \gg 50\%$, the thermal energy

18

444   during ramp heating likely becomes sufficiently high to increase the rate of the reaction. The

445   accumulation of additional thermal energy during the heating and cooling with increasing

446   MCT can thus be considered as a favorable factor promoting the decrease of the activation

447   energy near the end of dehydroxylation.

448

449   **Zero-order reaction and distribution of E_a values**

450   The zero-order reaction was observed in each heating cycle at the first step of

451   dehydroxylation for each sample. Zero-order kinetics implies that the reaction is

452   homogeneous and a portion of the non-dehydroxylated layers was transformed into

453   metakaolinite without formation of any intermediate phases, as found for 2:1 layer minerals

454   (Drits et al. 2011a,b, 2012a,b).

455   The KGa-2 sample is the best candidate to interpret the experimental data: its crystal

456   structure has a high density of stacking faults and the three particle size fractions have similar

457   structural disorder, as shown by almost identical the DTG and XRD patterns (Figs. 1a and 3a).

458   The DTG maximum temperatures of KGa-2 are significantly lower than those determined in

459   the TG screen patterns of KGa-1 and Keokuk samples, that corresponds to lower crystallite

460   thickness of KGa-2 kaolinite. With a low heating rate the small crystallites dehydroxylate

461   readily to produce a high rate of dehydroxylation (= low E_a) at relatively low temperatures T_P

462   and low degree of dehydroxylation DT_1 (Table 1). In contrast, the higher E_a is required to

463   dehydroxylate thicker crystallites. Therefore, in each heating cycle, the finest fraction of non-

464   dehydroxylated particles remaining after the previous heating cycle are dehydroxylated at the

465   interval of $M_S - M_P$ (where $\alpha < \alpha_p$). Thus, in each cycle of partial dehydroxylation, the

466   content of fine non-dehydroxylated particles is reduced. When $T_P > 440^oC$, however, the E_a

467   value drops significantly (Fig.10), even for the zero-order reaction and this result indicates

468   that at sufficiently high temperature, the reaction rate is controlled by both the structure of a

469   sample and by a high thermal energy accumulated by the sample during prior heating

19

470   intervals. Thermal energy accumulated by a sample results in of an increase in atomic

471   vibrations, especially hydrogen, to a degree where the stability decreases, and thus

472   dehydroxylation increases with lower activation energy.

473   Qualitatively, E_a values for KGa-1 and KGa-2 are similar to $T_P \sim 440^oC$. Indeed, at the

474   reaction onset the E_a values for both samples increase to their maximum values and then

475   decrease (Fig.10). The major differences between the E_a distributions are observed near the E_a

476   maxima at $T_P \sim 430\text{-}480^oC$, and probably results from the different particle and crystallite

477   sizes. The particles forming the second maximum of the bimodal distribution in KGa-1 are

478   larger than those dominating the entire KGa-2 sample and the crystallites are significantly

479   thicker, especially those in the coarser fraction (Fig.1b) . Therefore, within $430^oC < T_P <$

480   480^oC destabilization of layers related to atomic thermal vibrations is lower in KGa-1 than in

481   KGa-2, and the E_a values required to dehydroxylate the large crystallites are thus higher than

482   the E_a in KGa-2.

483   Within T_P from 430 to 530^oC, the curves of E_a evolution in Keokuk and KGa-1

484   samples are nearly parallel although for a given T_P, the E_a values in Keokuk are 3-5 kcal/mol

485   higher than those in KGa-1 (Fig. 10). The higher E_a in Keokuk sample is consistent with

486   greater crystallite thickness than that in the almost defect-free crystallites in KGa-1 (Figs. 1

487   and 2). Similar evolution of E_a over T_P for $T_P = 430\text{-}530^oC$ in Keokuk and KGa-1 implies a

488   qualitatively similar pattern of size distribution of defect-free crystallites in both samples.

489   Indeed, for a zero-order reaction, if the heating-cooling technique is applied to a population of

490   defect-free crystallites having a specific crystallite size distribution, the value of E_a in a

491   particular cycle is controlled entirely by the crystallite size of particles dehydroxylating in this

492   cycle. The evolution E_a values from cycle to cycle corresponds to the particle size distribution

493   (Drits et al. 2011a,b, 2012a). Thus, for two populations of defect-free crystallites having

494   different average crystallite sizes but similar crystallite size distribution shapes, the evolution

495   of E_a values should have two parallel distributions, with a difference in E_a for given T_p

20

496   reflecting the difference in absolute crystallite size between the populations. Therefore, the

497   observed similar distributions of E_a corresponding to dehydroxylation of defect-free

498   crystallites of different sizes in the Keokuk and the KGa-1, in combination with a similar

499   difference in E_a at a given T_p is explained by a similar distribution of crystallites in these

500   samples. The further increase of E_a with $T_p > 500ºC$ in the Keokuk sample is probably related

501   to the dehydroxylation of larger, highly ordered crystallites, responsible for the high

502   temperature DTG peaks observed in the TG screen pattern (Figure 3a).

503

504   **Second step of the reaction, at $\alpha > \alpha_p$**

505   The acceleration of reaction rate with T slows for each sample independent of

506   structural order, average particle size, and particle size distribution (Table 1, Figure 6). The

507   parameter n controls the decrease of acceleration or the deviation from the zero-order reaction.

508   The value of n increases with increasing DT_2, that is with an increase of the metakaolinite

509   content, although this relationship is not linear. Therefore, n parameter has similar values at

510   subsequent cycles of the same sample and yields close values for samples at similar DT_2

511   values but different MCT (Table 1; Fig. 11).

512   In each heating cycle, the activation energy of the first step of reaction, at $\alpha < \alpha_P$, is

513   higher than that of the second step, where $\alpha > \alpha_P$ (Table 1; Fig. 12). In KGa-2, the pattern of

514   E_a vs D_T is similar for curves corresponding to $\alpha < \alpha_P$ and $\alpha > \alpha_P$. In the Keokuk kaolinite,

515   the difference between E_a for $\alpha < \alpha_P$ and the E_a for $\alpha > \alpha_P$ of the same heating cycle (ΔE_a) is

516   high for the initial cycle of dehydroxylation and reaches maximum of ~ 13 kcal/mol at $D_T >$

517   20% and this value is maintained to the end of dehydroxylation. In KGa-1, the distribution of

518   E_a for $\alpha > \alpha_P$ follows the evolution of E_a for $\alpha < \alpha_P$ in the first cycles, similarly to KGa-2,

519   then E_a sharply decreases within D_T of 25-75%. The ΔE_a values yielded at $D_T < 40\%$ are in

520   the same range as the ΔE_a values observed in KGa-2 within the entire range of

21

521   dehydroxylation, whereas the ΔE_a maximum values reached at $D_T > 60\%$ are close to the ΔE_a

522   range of the Keokuk sample.

523   For each sample, n is low at the beginning of dehydroxylation, where the ΔE_a also is

524   low (Table 1; Fig. 11). The n parameter affects $Ln(d\alpha/dt)_a - Ln[(1-\alpha)^n/(1-n)]$ as the reaction

525   progresses at $\alpha > \alpha_P$. This effect is illustrated using the cycles of KGa-1 corresponding to

526   different n values. The $Ln(d\alpha/dt)$ curve at $\alpha > \alpha_P$ changes shape from cycle to cycle without a

527   apparent regularity (Figure 13). As shown above, each given α occurs at a fixed T_α and the

528   lower the $1-\alpha$, the lower the $1000/T_\alpha$ (Figure 8). Because in all cycles, α_P is fixed at a given

529   α, and α_P is similar in different cycles and samples (Table 1), the value of $Ln(1-\alpha)$ is nearly

530   the same for all cycles and samples. Subtraction of $Ln[(1-\alpha)^n/(1-n)]$ from $Ln(d\alpha/dt)_a$ at each

531   given α and $1000/T_\alpha$ results in two parts: the experimental $Ln(d\alpha/dt)$ and a straight line

532   corresponding to $Ln(f(T))$. The slope of $Ln(f(T))$ increases with n, in agreement with the

533   decrease of E_a found for these cycles (Figure 8). In general, however, the relationship between

534   the n and E_a values is not directly predictable because the observed n and DT_2 values are not

535   related by a linear relationship (Fig.11); E_a depends on the parameters α, n, and T_f. Therefore,

536   the actual E_a value is calculated using the experimental $Ln(d\alpha/dt)$ and $f(\alpha)$ (Equation 8).

537   Although metakaolinite contains very minor quantities of OH groups that may be

538   released at high temperature providing some mass loss (White et al. 2013), its contribution to

539   mass loss at $\alpha > \alpha_P$ would be negligible in respect to the mass loss provided by kaolinite

540   dehydroxylation. Therefore, it validates the kinetic model of mass loss at $\alpha > \alpha_P$ based

541   entirely on the dehydroxylation of kaolinite.

542

543   **Structural and morphological control on the two-step reaction model**

544   The structural integrity of layered minerals is partly determined by the thickness of

545   coherent scattering domains, CSDs, and each domain or crystallite requires a set of layers that

22

546   are strictly parallel. Large kaolinite particles usually consist of a set of crystallites, each

547   slightly disoriented with respect to a nearest neighbor. Therefore, the dehydroxylation reaction

548   involves the transformation of some crystallites to metakaolinite. As a result, the remaining

549   non-dehydroxylated crystallites may be encapsulated by metakaolinite formed owing to

550   dehydroxylation of the nearest crystallites, which suppresses the migration of H_2O molecules

551   out of the particle. The formation of metakaolinite that limits H_2O diffusion probably results

552   in a decrease in the reaction acceleration with an increase of dehydroxylation (Table 1), that is

553   in agreement of the model by Ortega et al. (2010).

554   Different structural and morphological features of each sample may have an influence

555   on the reaction rate of partial dehydroxylation at $\alpha > \alpha_P$. In KGa-1, for example, a sharp

556   decrease of the E_a is observed at $T_f > 449^oC$. Because, the crystallites composing the coarser

557   fraction (> 4 μm) of KGa-1 have a lower structural order than those in the finer (4-1 μm)

558   fraction (Fig. 1b), the presence of stacking faults in crystallites of the coarser fraction

559   probably decreases the attraction between the adjacent layers owing to the re-distribution of

560   hydrogen bonding between them. At high temperature (MCT $\geq 475^oC$) the presence of

561   stacking faults in combination with intense thermal atomic vibrations destabilizes kaolinite

562   layers and increases dehydroxylation.

563   The Keokuk kaolinite sample has large ΔE_a values with similar values for most cycles

564   (Table 1, Figure 12). A model is proposed where evolution of the total D_T over MCT shows

565   that a fraction of the total dehydroxylation in a given cycle, ΔD_T, increases from 2.4 to 9.0%

566   for the first four cycles. Following cycles from 9 to13 have ΔD_T within narrow range from

567   9.0% to 13.1% with average value equaled to 11.6% (Table 1). For the first four cycles the E_a

568   values decrease in the first and the second steps with increasing of the cycle number. The

569   decrease of E_a during first step most probably is related to a presence of some stacking faults

570   in dehydroxylated crystallites. In contrast, the E_a values increase in both steps with increasing

571   cycle number from 9 to13 (Table 1). The ΔE_a values in these cycles are also quite constant,

23

572   following the ΔD_T (Table 1; Figure 12). Therefore, the same portion of crystallites having

573   similar size is probably subjected to dehydroxylation in both the first ($\alpha < \alpha_P$) and second (α

574   $> \alpha_P$) steps of the same heating cycle. During the first step of partial dehydroxylation, some

575   layers of these large crystallites are transformed into metakaolinite. Therefore, at $\alpha \approx \alpha_P$, the

576   non-dehydroxylated parts of the crystallites containing stacking faults are expected to become

577   thinner and during the second step of dehydroxylation the reaction thus occurs at higher rate

578   and lower activation energy (Table 1, cycles 6 to 9). In contrast, in cycles 9-13 the relative

579   degree of dehydroxylation during the first step (DT_1) is about twice lower than that during the

580   second step (DT_2) (Table 1). In addition, relatively to the first step, a non-dehydroxylated

581   portion reacting during the second step ($DT_2 - DT_1$) of a cycle is lower than that

582   dehydroxylated during the second step in each following cycle (Table 1). As a result, the

583   activation energy required to dehydroxylate a larger, non-dehydroxylated part during the

584   second step of the reaction increases in each following cycle. Fractions of the relative degree

585   of dehydroxylation for the first (ΔDT_1) and the second steps (ΔDT_2) in cycles 9-13 vary within

586   narrow ranges, from 3.4% to 4.3%, and from 6.4% to 10.8%, respectively (Table 1). As a

587   result, in cycles 9-13, the E_a values for both the first and second steps vary only little between

588   the subsequent cycles, differing within a narrow range from 0.5 to 1.7 kcal/mol, thus

589   providing similar ΔE_a in subsequent the cycles (Table 1).

590   The XRD patterns (Fig.1 a,b) and DTG patterns (Fig. 3a,b) obtained for the two

591   dominant fractions of the KGa-2 sample show that crystallites have high stacking disorder but

592   the same thickness and, thus, they have a homogeneous composition. In addition, these

593   crystallites are smaller and thinner than those of the other samples. Therefore, the increase of

594   the ΔE_a value depends mostly on the n value, which controls the slowing of the acceleration of

595   the reaction rate during the second step of the reaction. Indeed, a strong correlation exists in

596   increasing ΔE_a versus n (Table 1).

597   Remarkably, in all samples studied, the *n* value is low or zero at the beginning of

598   dehydroxylation, where metakaolinite incompletely surrounds kaolinite, non-dehydroxylated

599   crystallites (Fig. 12). The suppression mechanism occurs by diffusion along grain and phase

600   boundaries. The higher the contribution of diffusion suppression by metakaolinite, the greater

601   the *n* parameter.

602   The two-step mechanism of kaolinite dehydroxylation derived from the heating-

603   cooling experiments remain in perfect agreement with the model by Ortega et al. (2010) who

604   introduced the two-step mechanism using an isoconversional technique of kinetics

605   determination. The first step postulated by Ortega et al. (2010) corresponds to a nucleation of

606   metakaolinite followed by nuclei growth. The dehydroxylation begins from grain edges and

607   progresses parallel to the (001) planes. In the second step of reaction, in advanced

608   dehydroxylation, metakaolinite closes the intralamellar channels leaving kaolinite portions

609   encapsulated, where H_2O molecules diffusion is suppressed. The two-step reaction of

610   kaolinite dehydroxylation was also found by Frost and Vassello (1996) from the infrared

611   spectroscopy data and by Otero-Arean et al. (1982) who determined a two-step reaction using

612   NMR data, where the first reaction occurred *via* layer-by-layer transformation.

613

614   **Apprarent meaning of the activation energy of partial dehydroxylation**

615   In numerous studies on dehydroxylation of dioctahedral phyllosilicates the calculated

616   absolute values of E_a strongly depend on the method applied and the measurement conditions

617   (Vyazovkin et al. 2011), making the E_a values hardly comparable between different studies

618   (Ptáček et al. 2011 and Drits et al. 2012a, and references therein). Therefore, the E_a values

619   obtained here cannot be compared to those determined by isoconversional, isothermal, or non-

620   isothermal methods. The values are also not comparable to the E_a calculated from a protocol

621   where the dehydroxylation of kaolinite occurs over the entire reaction and involves all

622   particles of the sample in the dehydroxylation process. In contrast, the heating and cooling

25

623   experiment provide reaction selectivity using previously non-dehydroxylated crystallites in a

624   given heating cycle. The E_a values obtained from the heating and cooling experiments depend

625   on the particular heating and cooling protocol applied. Using the same protocol, however, E_a

626   values obtained for different cycles and samples are comparable and can be used for reliable

627   interpretation of mechanism of dehydroxylation (Drits et al. 2012a). Although different

628   protocols than the applied in the present study will result in different values of kinetic

629   parameters, the general mechanism of partial dehydroxylation of kaolinite should be the same

630   and a two-step reaction is expected (compare to Ortega et al. 2010).

631

632

633   **Implications for dehydroxylation of phyllosilicates and related minerals**

634   Firing clays to produce ceramics is the oldest and most widespread reaction of

635   dehydroxylation among human activities. Despite numerous studies devoted to kinetic

636   dehydroxylation of phyllosilicates, including kaolinites, there is no general agreement

637   concerning a rate-controlling mechanism of the reaction. A possible reason is that

638   dehydroxylation has been studied as a continuous reaction, from the beginning to the end, in

639   one heating event, ignoring a possible co-existence of multi-steps discrete kinetics. Novel

640   archeological dating method based on the rate of rehydroxylation determined for kaolinite-

641   rich ceramic artifacts should take into account the kaolinite behavior after possibly incomplete

642   dehydroxylation due to insufficient firing (Clegg et al. 2012).

643   A multi-cycle heating and cooling TG technique is a powerful tool to investigate the

644   evolution of kinetic behavior and structural transformation of a sample subjected to thermal

645   treatment at different stages of its partial dehydroxylation and was found successful for a new

646   insight into the nature of dehydroxylation-rehydration processes in dioctahedral 2:1 clay

647   minerals (Drits and McCarty 2007; Drits et al. 2011a,b, 2012a; Derkowski et al. 2012).

648   Moreover, because structural studies of dehydroxylation (using XRD, infrared spectroscopy,

26

649   solid-state nuclear magnetic resonance) involve an analysis that is usually performed on

650   partially dehydroxylated samples, not within a continuous heating reaction, the results of a

651   heating-cooling TG experiment is more comparable to the structural study than a conventional

652   kinetic analysis. Therefore the heating and cooling technique in combination with different

653   structural methods should lead to a consistent model of kinetical and structural behavior of a

654   mineral at different stages of its partial dehydroxylation providing unambiguos interpretation

655   of the experimental data. This technique is thus recommended to study thermal reactions and

656   structural transformation of various minerals. It can be especially useful to determine thermal

657   stability of pillared clays and organic-minerals nanocomposites that are usually calcined at

658   various temperatures (i.e. partially dehydroxylated) prior to structural analyses and

659   applications (e.g., Aceman et al. 1997; Cheng et al. 2012).

660   The multi-cycle TG method considers partial dehydroxylation of kaolinite samples

661   with stacking order-disorder, average particle size, and the particle size distribution. For the

662   first time it is shown that each stage of partial dehydroxylation consists of two subsequent

663   processes with different kinetic parameters describing the reaction rate. The first step

664   corresponds to a zero-order reaction indicating that the reaction is homogeneous and a non-

665   dehydroxylated layer is transformed into metakaolinite layer without a formation within the

666   layer of domains differing by degree of dehydroxylation. During the second step of the same

667   cycle of partial dehydroxylation the acceleration of reaction rate with temperature is

668   suppressed because metakaolinite delays the immediate diffusion H_2O molecules out of the

669   crystallite.

670   The interpretation derived from the observed evolution of kinetic parameters for the

671   samples of distinctively different structural and morphological features predicts that their

672   partially dehydroxylated varieties can consist of crystallites formed by coexisting non-

673   dehydroxylated layers and metakaolinite layers. These coexisting layers can form an

674   interstratified structure, as was predicted for the dioctahedral 2:1 clay minerals using by the

27

675   multi-cycle TG method and proven with structural studies (Drits et al. 2011a, 2012a,b).Such

676   unusual interstratified structures formed among partially dehydroxylated dioctahedral clays

677   may have useful properties.

678   Besides the 2:1 layer dioctahedral minerals (mostly illite, smectite and mixed-layered

679   illite-smectite) and chlorite, kaolinite mineral group is the most widespread clay mineral in the

680   Lithosphere, involved in a variety of natural reactions. Among all minerals on Earth, kaolinite

681   contains the highest fraction of OH that can be released at high temperature as H_2O; roughly

682   three times more than in common micas. With lower activation energy than in mica, and far

683   greater quantity of released water, dehydroxylation of kaolinite occurring during frictional

684   heating upon earthquakes is the more efficient reaction than the dehydroxylation of mica,

685   providing large quantities of water that decrease the effective normal stress and reduces the

686   faults propagation (Hirono and Tanikawa, 2011). The pathway of kaolinite dehydroxylation

687   affects, however, the calculation of absorbed energy.

688

696

697

28

698   **References**

699

700   Aceman, S., Lahav, N., and Yariv, S. (1997) XRD study of the dehydration and rehydration

701   behaviour of Al-pillared smectites differing in source of charge. Journal of Thermal

702   Analysis, 50, 241-256.

703   Cheng, H., Liu, Q., Cui, X., Zhang, Q., Zhang, Z., and Frost, R.L. (2012) Mechanism of

704   dehydroxylation temperature decrease and high temperature phase transition of coal-

705   bearing strata kaolinite intercalated by potassium acetate. Journal of Colloid and

706   Interface Science, 376, 47–56

707   Hirono, T., and Tanikawa, W. (2011) Implications of the thermal properties and kinetic

708   parameters of dehydroxylation of mica minerals for fault weakening, frictional

709   heating, and earthquake energetic. Earth and Planetary Science Letters, 307, 161-172.

710   Clegg, F., Breen, C., Carter, M.A, Ince, C., Savage, S.D., and Wilson, M.A. (2012)

711   Dehydroxylation and Rehydroxylation Mechanisms in Fired Clay Ceramic: A TG-MS

712   and DRIFTS Investigation. Journal of the American Ceramic Society, 95, 416–422.

713   Bailey, S.W. (1988) Polytypism of 1:1 layer silicates. In S.W.Bailey, Ed., Hydrous

714   phyllosilicates (Exclusive of Micas), p. 9-27. Reviews in Mineralogy, Mineralogical

715   Society of America, Chantilly, Virginia.

716   Bish, D.L. (1993) Rietveld refinement of the kaolinite structure at 1.5 K. Clays and Clay

717   Minerals, 41, 738-744.

718   Bish, D.L., and van Dreele, R.B. (1989) Rietveld refinement of non-hydrogen atomic

719   positions in kaolinite. Clays and Clay Minerals, 37, 289-296.

720   Bookin, A.S., Drits, V.A., Plançon, A., and Tchoubar, C. (1989) Stacking faults in kaolin-

721   group minerals in the light of real structural features. Clays and Clay Minerals, 37,

722   297-307.

29

723   Brindley, G.W., Chin-Chun, K., Harrison, J.L., Lipsicas, M., and Raythatha, R. (1986)

724   Relationship between structural disorder and other characteristics of kaolinites and

725   dickites. Clays and Clay Minerals, 34, 239-249.

726   Brindley, G.W. and Nakahira, M. (1957) Kinetics of dehydroxylation of kaolinite and

727   halloysite. Journal of the American Ceramic Society, 40, 346-350.

728   Brindley, G.W., and Roberson, K. (1946) The structure of kaolinite. Mineralogical Magazine,

729   72, 242-253.

730   Derkowski, A., Drits, V.A., and McCarty, D.K. (2012) Nature of rehydroxylation in

731   dioctahedral 2:1 layer clay minerals. American Mineralogist, 97, 610-629.

732   Drits V.A., and McCarty, D.K. (2007) The nature of structure-bonded H_2O in illite and

733   leucophyllite from dehydration and dehydroxylation experiments. Clays and Clay

734   Minerals, 55, 45-58.

735   Drits, V.A., Derkowski, A., and McCarty, D.K. (2011a) New insight into the structural

736   transformation of partially dehydroxylated pyrophyllite. American Mineralogist, 96,

737   153-171.

738   Drits, V.A., Derkowski, A., and McCarty, D.K. (2011b) Kinetics of thermal transformation of

739   partially dehydroxylated pyrophyllite. American Mineralogist, 96, 1504-1069.

740   Drits, V.A., Derkowski, A. and McCarty, D.K. (2012a) Kinetics of partial dehydroxylation in

741   dioctahedral 2:1 layer clay minerals. American Mineralogist, 97, 930-950.

742   Drits, V.A., McCarty, D.K., Derkowski, A. (2012b) Mixed-layered structure formation during

743   trans-vacant Al-rich illite partial dehydroxylation. American Mineralogist, 97, 1922-

744   1938.

745   Dubois, J., Mura,t M., Amroune, A., Carbonneau, X., and Gardon, R. (1995). High

746   temperature transformation in kaolinite: the role of crystallinity and the firing

747   atmosphere. Applied Clay Science, 10, 87-98.

30

748   Franco, F., Pérez-Maqueda, L.A., and Perez-Rodriguez, J.L. (2003) The influence of

749   ultrasonic on the thermal behavior of well-ordered kaolinite. Thermochimica Acta,

750   404, 71-79.

751   Franco, F., Pérez-Maqueda, L.A., and Perez-Rodriguez, J.L. (2004) The effect ultrasonic on

752   the partical size distribution and structural disorder of well-ordered kaolinite. Journal

753   of Colloid and Interface Science, 274, 101-107.

754   Frost, R.L., and Vassallo, A.M. (1996) The dehydroxylation of the kaolinite clay minerals

755   using infrared emission spectroscopy. Clays and Clay Minerals, 44, 635-651.

756   Kogure, T., and Inoue, A. (2005) Determination of defect structures in kaolin minerals by

757   high-resolution transmission electron microscopy (HRTEM). American Mineralogist,

758   90, 85-89.

759   Kogure, T., Johnston, C.T., Kogel, J.E., and Bish, D.L. (2010) Stacking disorder in a

760   sedimentary kaolinite. Clays and Clay Minerals, 58, 63-72.

761   MacKenzie, K.J.D., Brown, I.W.M., Meinhold, R.H., and Bowden, M.E. (1985) Outstanding

762   problems in the kaolinite-mullite reaction sequence investigated by ^{29}Si and ^{27}Al solid-

763   state nuclear magnetic resonance: I metakaolinite. Journal of the American Ceramic

764   Society, 68, 293-297.

765   Ortega A., Rouquerol F., Akhouayri S., Laureiro Y. and Bouquerol J. (1993) Kinetical study

766   of the thermo-analysis of kaolinite between 30°C to 1000°C by controlled rate evolved

767   gas analysis. Applied Clay Science, 8, 207-214.

768   Ortega A., Macias M., and Gotor F.J. (2010) The multistep nature of the kaolinite

769   dehydroxylation: kinetics and mechanism. Journal of the American Ceramic Society,

770   93, 197-203.

771   Otero-Arean, C., Letellier, M., Gersteinand, J.J., and Fripiat, B.G. (1982) Protonic Structure

772   of Kaolinite During Dehydroxylation Studied by Proton Nuclear Magnetic Resonance.

773   Bulletin de Minéralogie, 105, 499-508.

31

774 Pérez-Maqueda, L.A., Criado, J.M., and Sánchez Jiménez, P.E (2006) Combined kinetic

775   analysis of solid-state reactions: a powerful tool for the simultaneous determination of

776   kinetic parameters and the kinetic model without previous assumptions on the reaction

777   mechanism. Journal of Physical Chemistry A, 110, 12456-12462.

778 Plançon, A., Giese, R.F., Snyder, R., Drits, V.A., and Bookin, A.S. (1989) Stacking faults in

779   the kaolin-group mineral-defect structures of kaolinite. Clays and Clay Minerals, 37,

780   203-210.

781 Ptáček, P., Opravil, T., Šoukal, P., Wasserbauer, J., Másilko, J., and Baráček, J. (2013) The

782   influence of structural order on kinetic dehydroxylation of kaolinite. Journal of the

783   European Ceramic Society, 33, 2793-2799.

784 Ptáček, P., Šoukal P., Opravil, T., Havilica, J., and Brandstetr, J. (2011) The kinetic analysis

785   of the thermal decomposition of kaolinite by DTG technique. Powder Technology,

786   204, 20-25.

787 Sestak J., and Berggren G. (1971) Study of the kinetics of the mechanism of solid-state

788   reactions at increased temperature. Thermochemica Acta, 3, 1-12.

789 Slonimskaya, M.V., Drits, V.A., Finko, V.I., and Salyn, A.L. (1978) The nature of interlayer

790   in fine-dispersed muscovites. Izvestiya Akademii Nauk SSSR, seriya geologicheskaya,

791   № 10, 95-104 (in Russian).

792 Vyazovkin, S., Burnham, A.K., Criado, J.M., Pérez-Maqueda, L.A., Popescu, C., and

793   Sbirrazzuoli, N. (2011) ICTAC Kinetics Committee recommendations for performing

794   kinetic computations on thermal analysis data. Thermochimica Acta, 520, 1-19.

795 Wardle, R., and Brindley, G.W. (1972) The crystal structure of pyrophyllite, 1Tc, and its

796   dehydroxylate. American Mineralogist, 57, 732-750.

797 White, C.E., Kearley, C.J., Provis, J.L., and Riley, D.P. (2013) Inelastic neutron scattering

798   analysis of the thermal decomposition of kaolinite to metakaolinite. Chemical Physics,

799   427, 82-86.

800   White, C.E., Kearley, C.J., Provis, J., Proffen, T., Riley, D.P., and van Denver, S.J. (2010)

801   Density functional modeling of the local structure of kaolinite subjected to thermal

802   dehydroxylation. Journal of Physical Chemistry A, 114, 4988-4996

803   Yeskis, D., Koster van Groos, A.F.K., and Guggenheim, S. (1985) The dehydroxylation of

804   kaolinite. American Mineralogist, 70, 159-164.

805

806 **Figure captions:**

807 Figure 1. X-ray diffraction (XRD) patterns of studied samples in random (disoriented) powder

808 form: (a) bulk samples, (b) particle size fractions of 1-4 µm (gray) and > 4 µm (black).

809 Figure 2. Particle size distribution (PSD) measured for bulk samples studied. Note the

810 logarithmic particle size scale on the horizontal axis.

811 Figure 3. Thermogravimetric (TG) analysis patterns of the samples studied; TG mass loss and

812 mass change (DTG) curves. (a) TG and DTG curves for bulk samples analyzed with a

813 2ºC/min heating rate; values given in % correspond to the total mass loss in the

814 temperature range as presented on the horizontal axis; (b) DTG curves for the particle

815 size fractions of KGa-1 and KGa-2 samples, recorded with a 5ºC/min heating rate.

816 Values given above the curves correspond to temperature of DTG maxima. Note

817 different heating rates in (a) and (b).

818 Figure 4. TG, DTG, and temperature evolution curves for bulk samples subjected to heating-

819 cooling multi-cycle experiments. Numbers presented above the temperature curve at

820 local maxima correspond to the heating cycle number in Table 1.

821 Figure 5. A portion of Figure 4 presenting details for a single cooling-heating cycle,

822 representative for (a) the part of experiment at low degree of dehydroxylation, i.e.

823 KGa-2, cycle 6, (b) the part of experiment at high degree of dehydroxylation, i.e. KGa-

824 2, cycle 9. See the text for labels description. Note the different shape of the DTG

825 curves and different position of M_f in the (a) and (b).

826 Figure 6. The $Ln(d\alpha/dt)$ over $1000/T$ plotted with all points within the M_S-M_f range for the

827 cycles corresponding to the intense dehydroxylation; compare to Figures 4 and 5.

828 Figure 7. Plots of $Ln(d\alpha/dt)$ over α overlapped with the curves of $Ln(d\alpha/dt)$ over $1000/T$ given

829 for selected representative cycles presenting the estimation of α_P. The point of

830 deviation in the $Ln(d\alpha/dt)$ over $1000/T$ from the straight trend line corresponds to a

831 certain α that becomes α_P.

34

832   Figure 8. The plots of the experimental $Ln(d\alpha/dt)$, $Ln(f(T))$, and calculated $Ln[(1-\alpha)^n/(1-n)]$

833   functions over $1000/T$ (left and middle plots) and over α (right) for two representative

834   cycles of KGa-1 samples, given as an example of the influence of the n parameter on

835   the deviation from linearity of $Ln(d\alpha/dt)$ over $1000/T$ (Equation 9). Note different n

836   values in the cycles presented.

837   Figure 9. The cycle-change (Δ) of degree of dehydroxylation calculated separately based on

838   the mass loss in the part of each cycle at $\alpha < \alpha_P$ (DT_1, Equation 10a) and for the part of

839   each cycle at $\alpha > \alpha_P$ (DT_2, Equation 10b). The ΔDT_1 and ΔDT_2 values are plotted in a

840   function of T_P (left) and T_f (right), respectively, corresponding to the end temperature

841   for a given step in a cycle. See Figure 5. Note a different vertical scale in the plots.

842   Figure 10. Activation energy (E_a) values calculated separately for the range of $\alpha < \alpha_P$ (left)

843   and $\alpha > \alpha_P$ (right), using different kinetic models (equations 7 and 8, respectively),

844   plotted in a function of T_P and T_f, respectively. Compare to Figure 9. Note a different

845   vertical scale in the plots.

846   Figure 11. The value of parameter n (Equation 8) plotted as a function of DT_2 (Equation 10b)

847   for the kinetic reaction at $\alpha > \alpha_P$ (Table 1).

848   Figure 12. Activation energy (E_a) values calculated separately for the range of $\alpha < \alpha_P$ and $\alpha >$

849   α_P at each cycle, using different kinetic models (equations 7 and 8, respectively),

850   plotted over total degree of dehydroxylation (D_T, Equation 6). ΔE_a represents a

851   difference in E_a between the step at $\alpha < \alpha_P$ and the step at $\alpha > \alpha_P$ in a given cycle.

852   Figure 13. The evolution of experimental $Ln(d\alpha/dt)$ (left) and calculated $Ln[(1-\alpha)^n/(1-n)]$

853   (right) over $1000/T$ curves given for the step at $\alpha > \alpha_P$ for representative cycles of

854   dehydroxylation in the KGa-1 sample.

35

Keokuk

KGa-1

KGa-2

°2Θ CuKα

Figure 1a

Gray - fractions 1-4 µm
Black - fractions > 4 µm

KGa-2

KGa-1

Keokuk

°2Θ CuKα

Figure 1b

Figure 2

KGa-2   460   13.5%

KGa-1   479   569   13.5%

Keokuk   641   663   598   476   13.6%

Temperature (ºC)

Figure 3a

KGa-2   497 503

KGa-1   509 513   534   644

fractions > 4 µm
fractions1 - 4 µm
fractions < 1 µm

Temperature (ºC)

Figure 3b

KGa-2

TG curve

DTG curve

Temperature
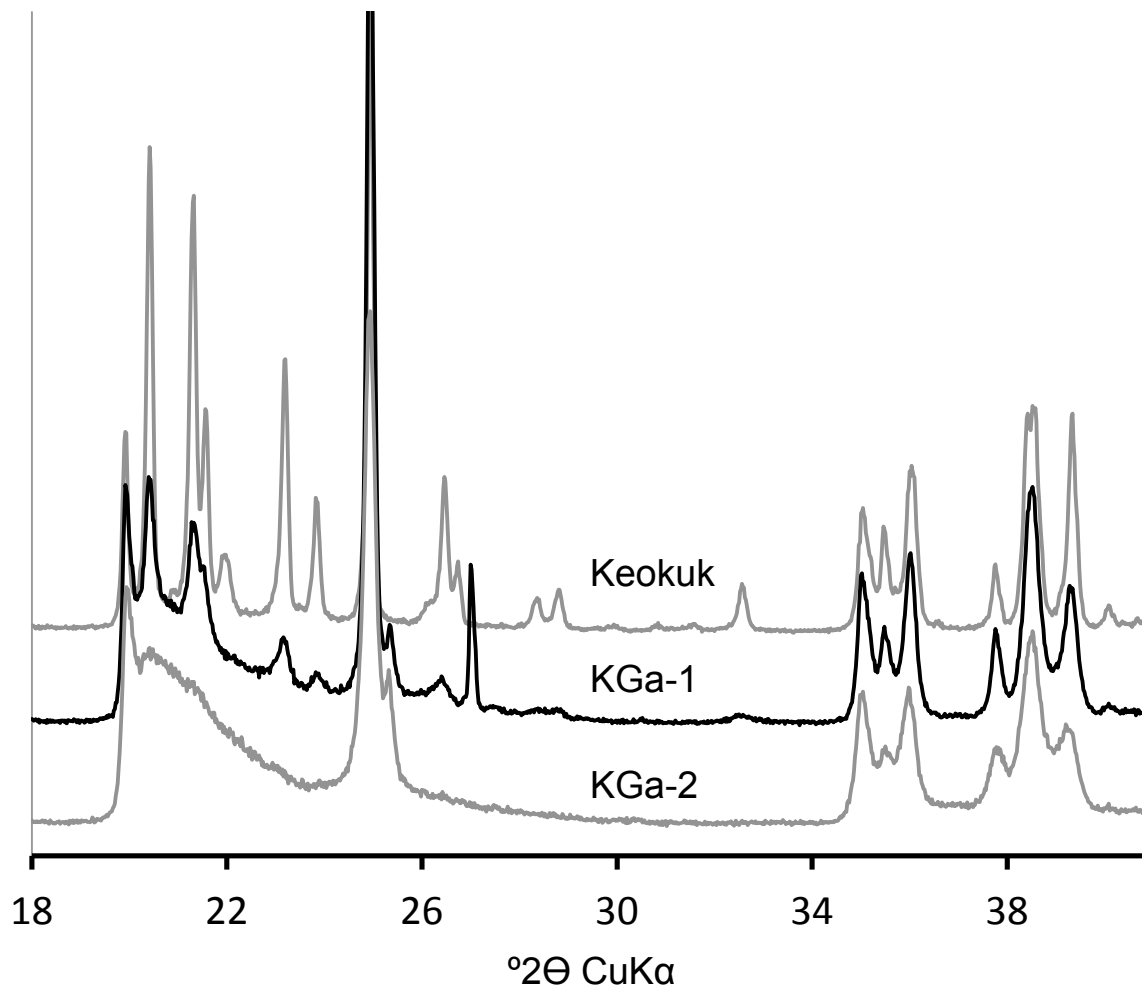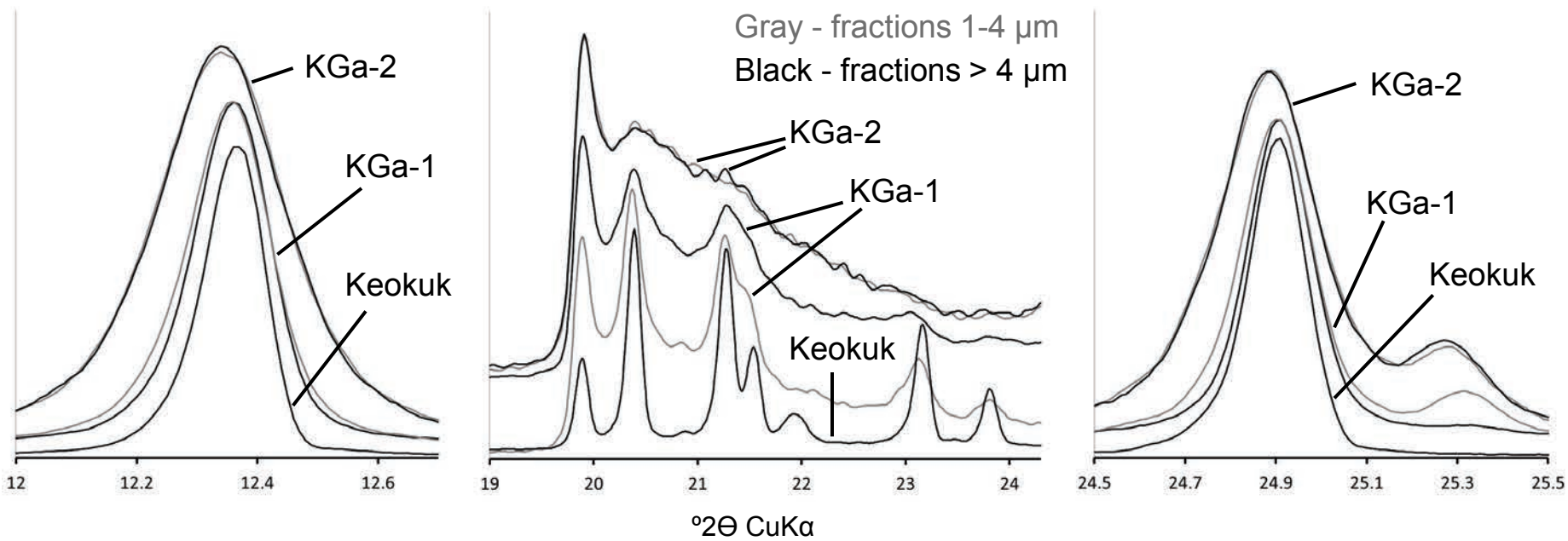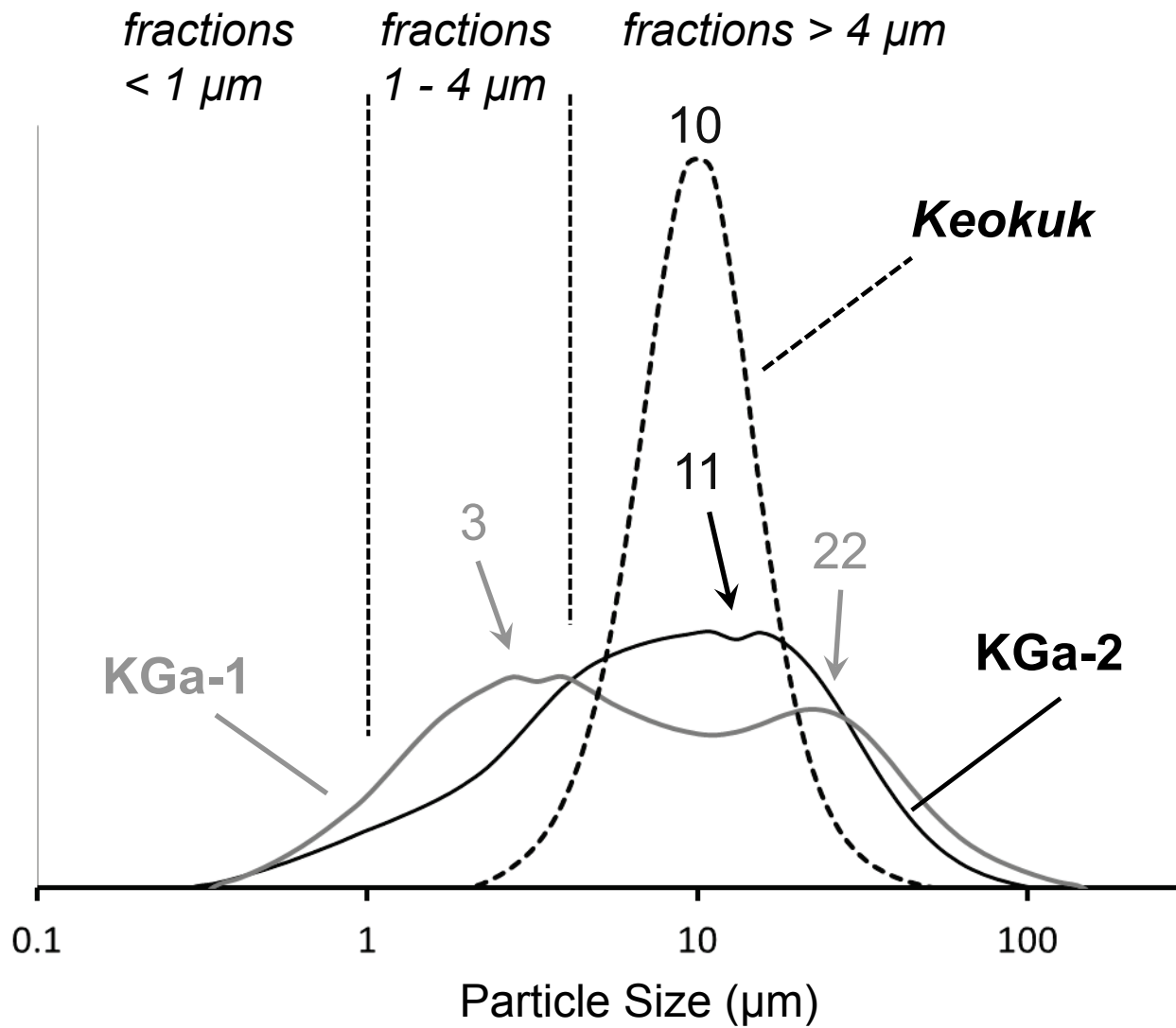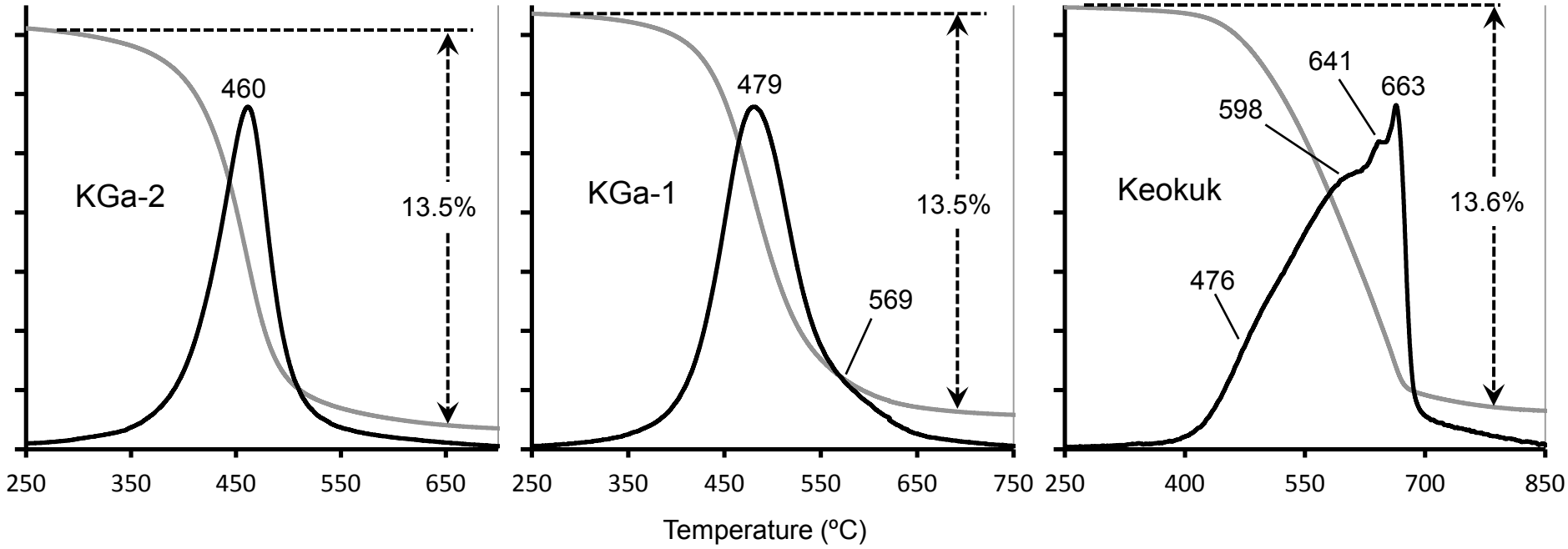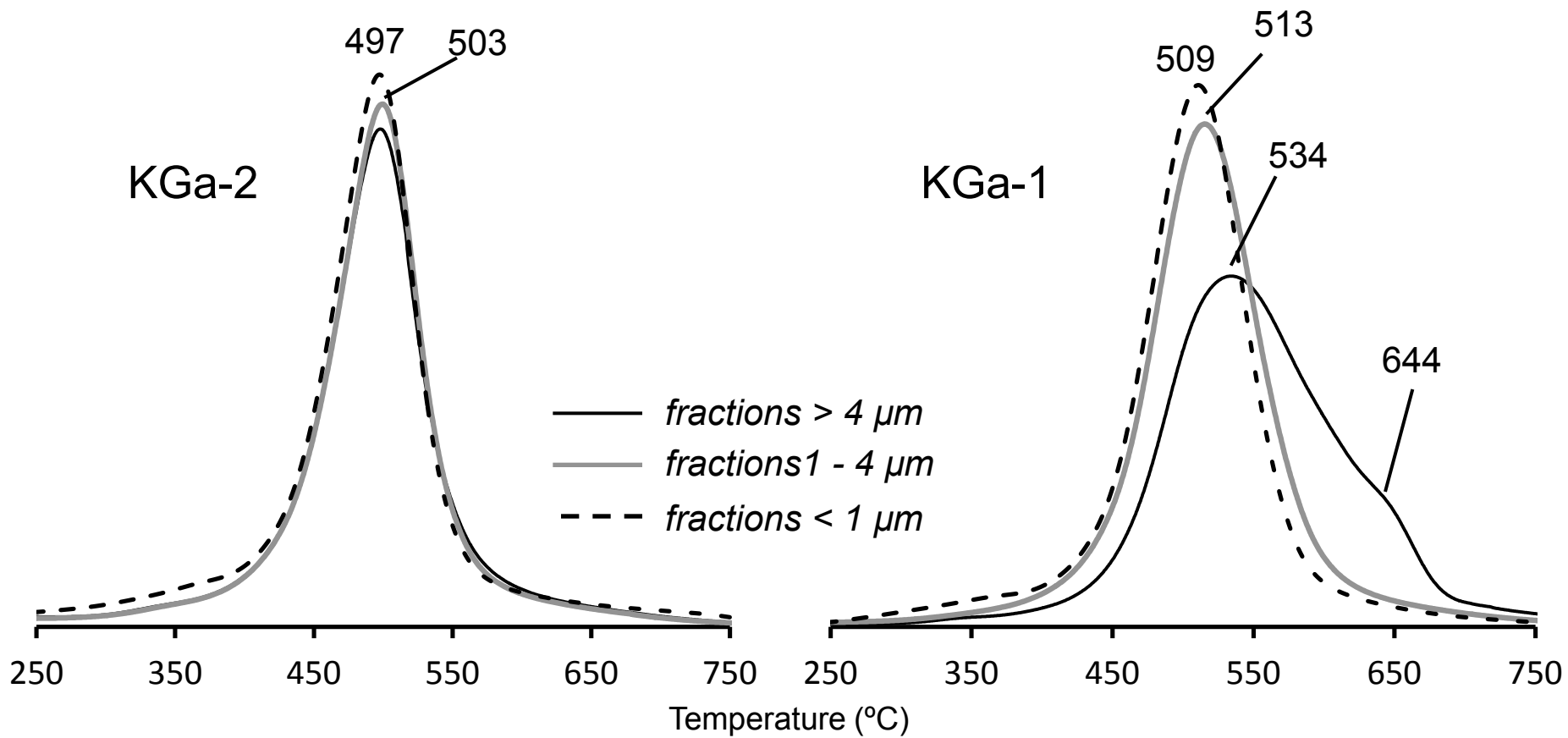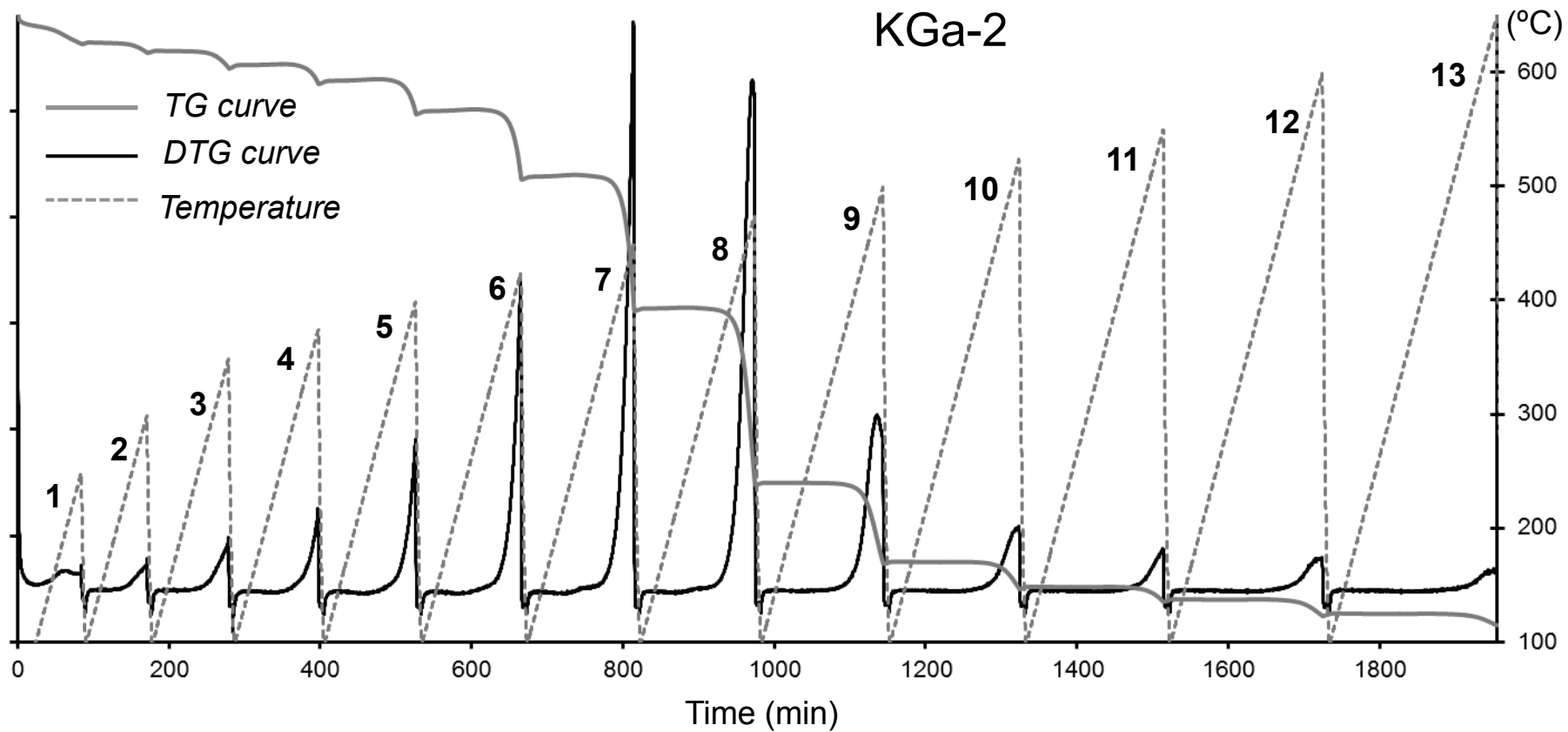
Figure 4 (panel 1)

Figure 4 (panel 2)

Keokuk
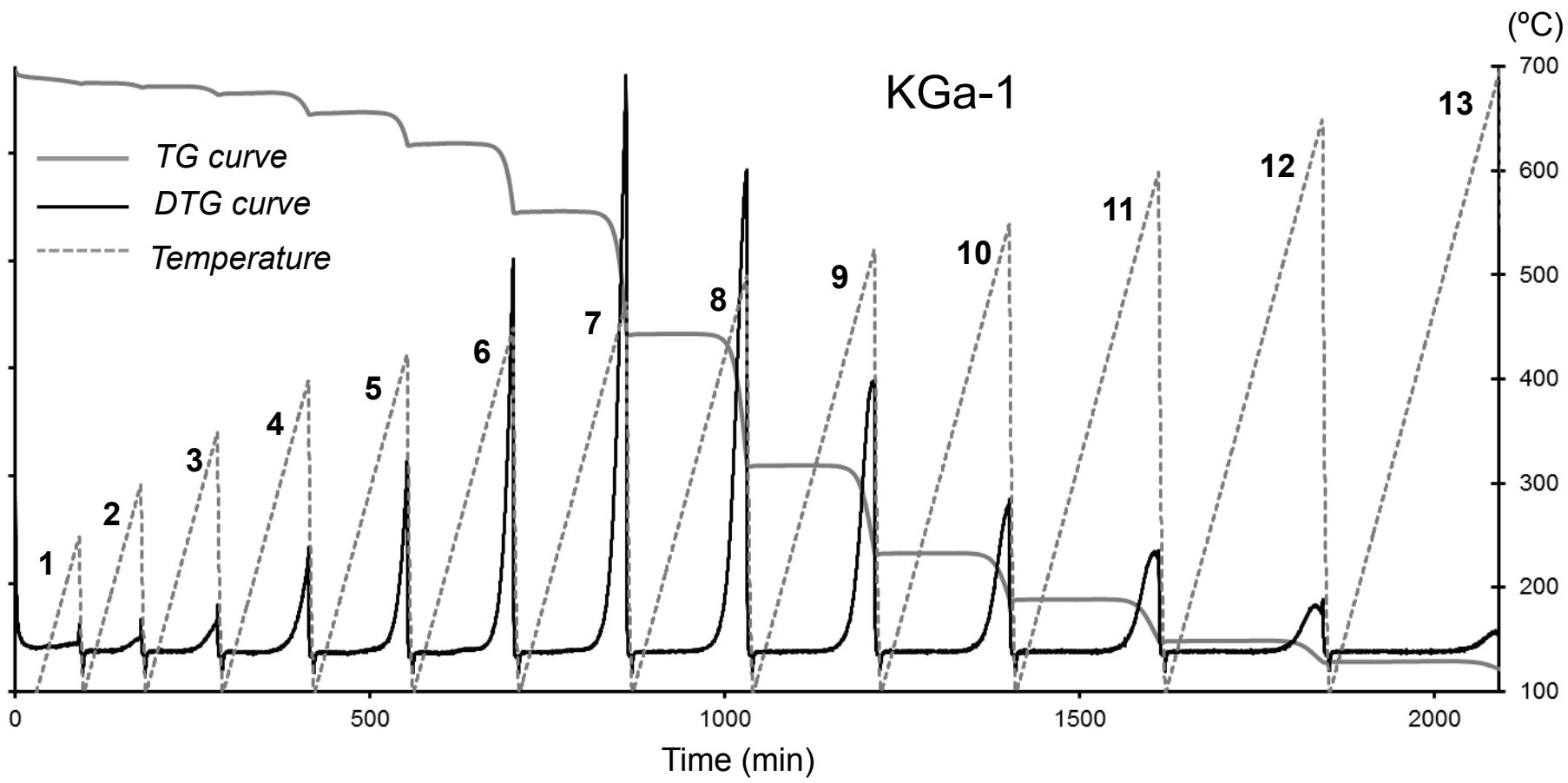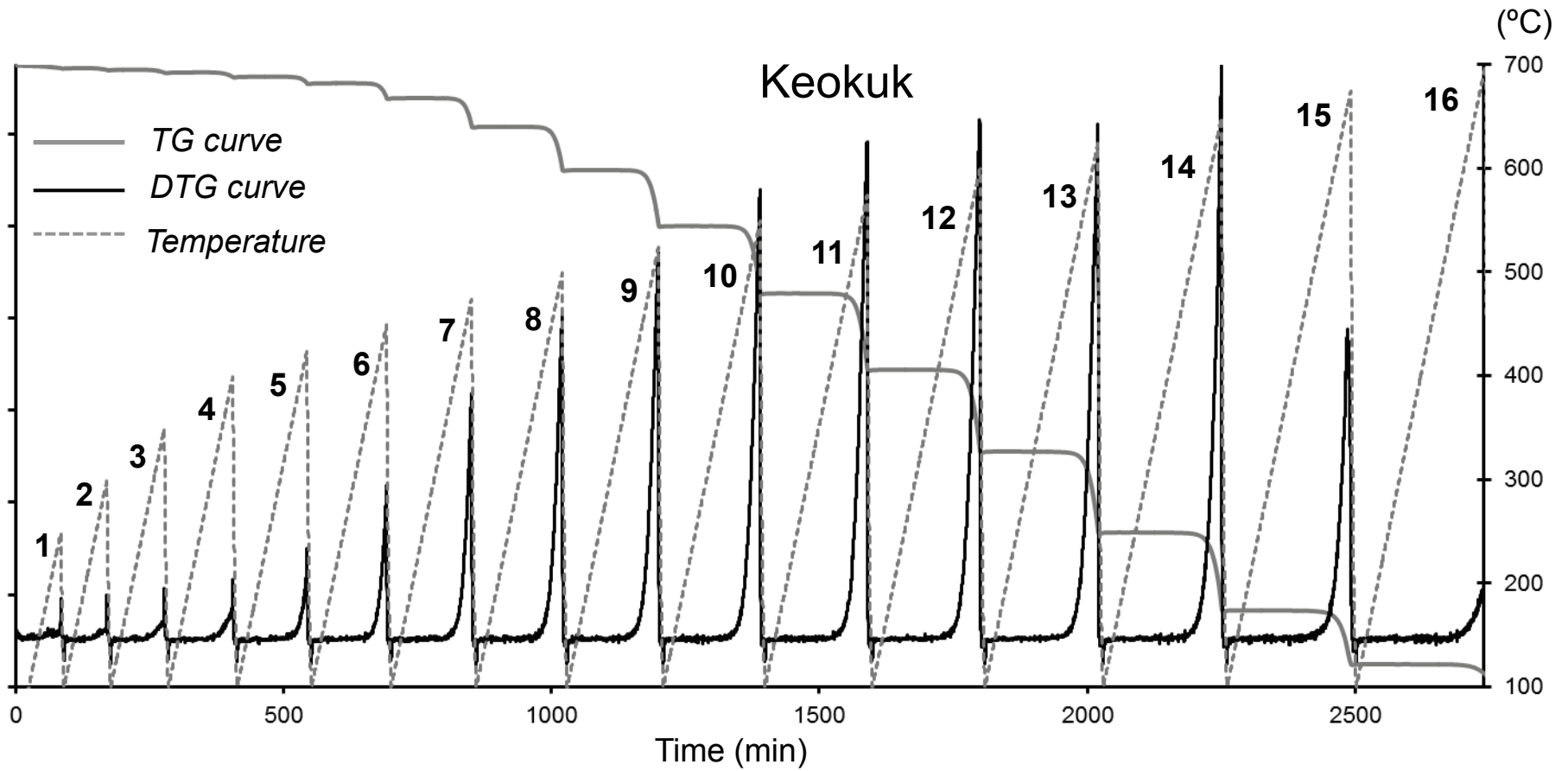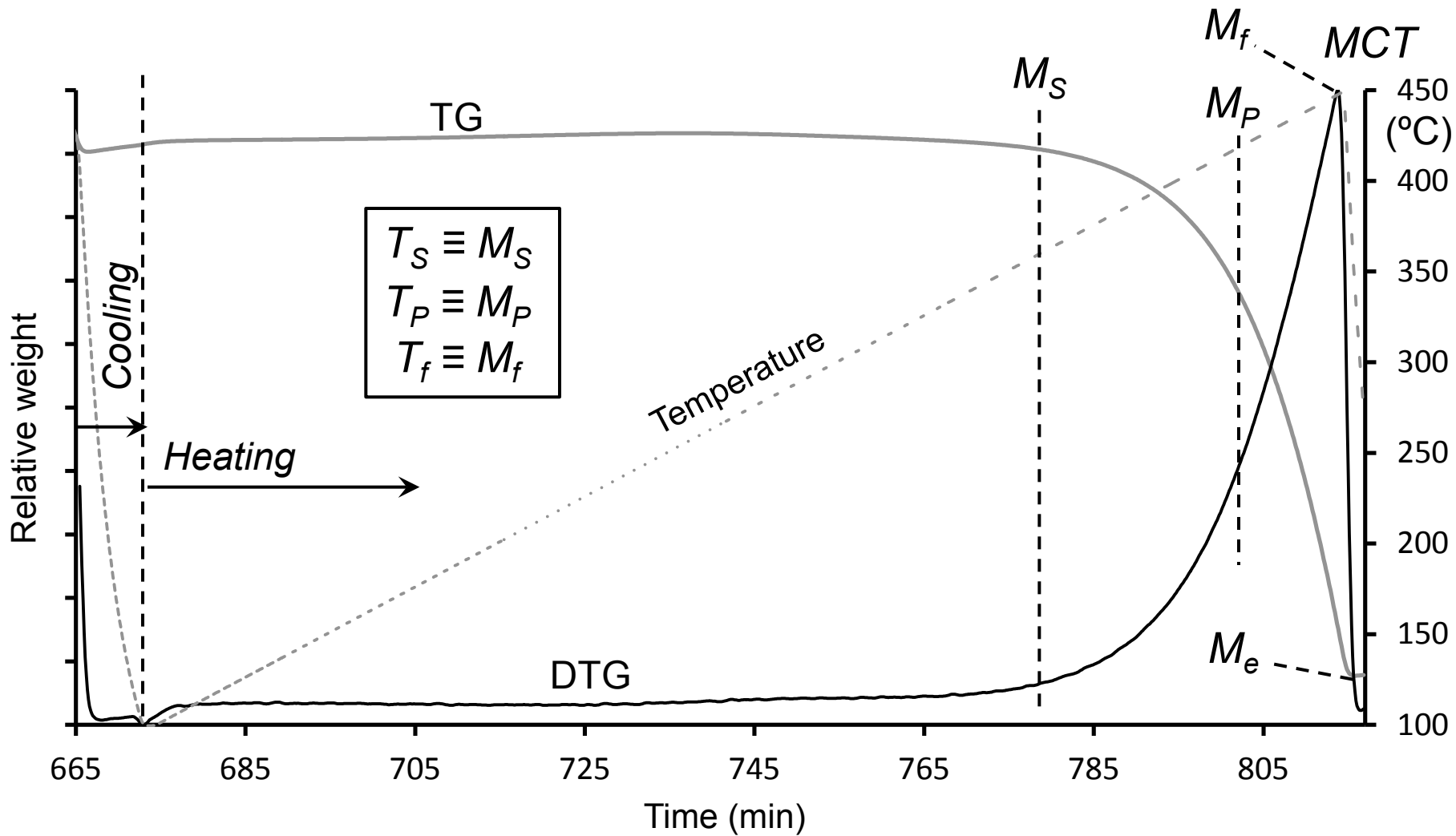
Figure 4 (panel 3)

Figure 5a
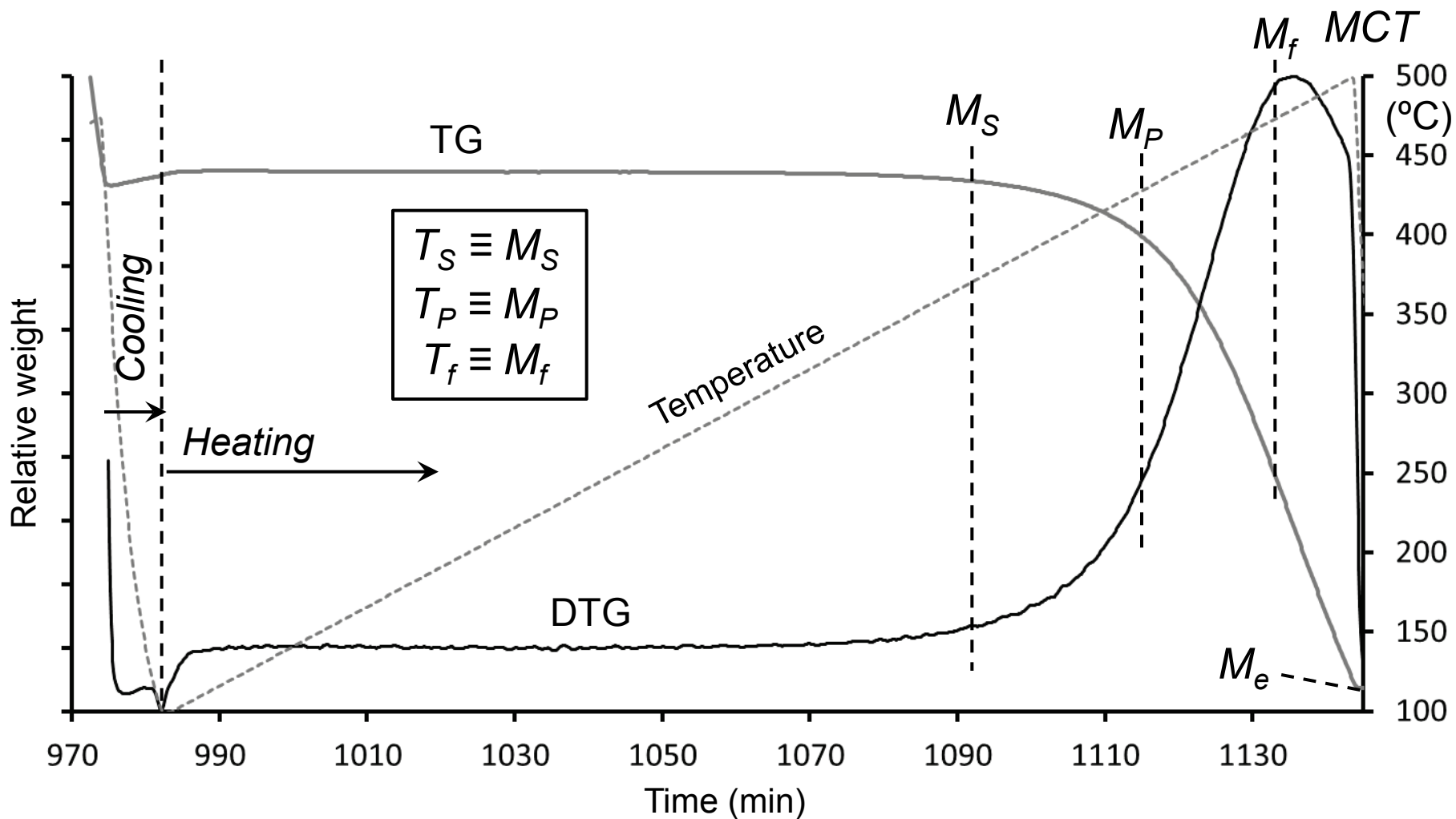
Figure 5b
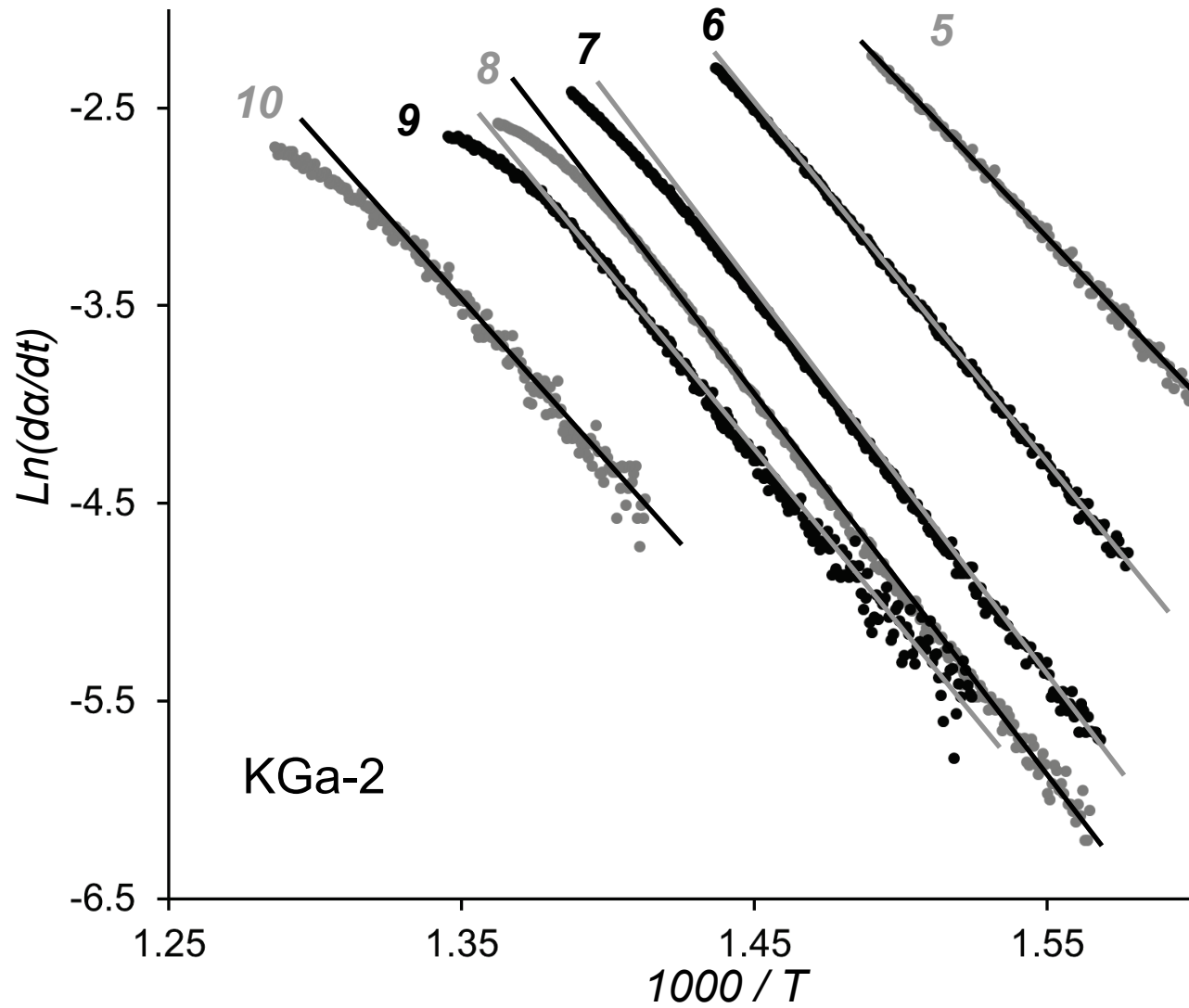
Figure 6 (panel 1)

Figure 6 (panel 2)

Keokuk
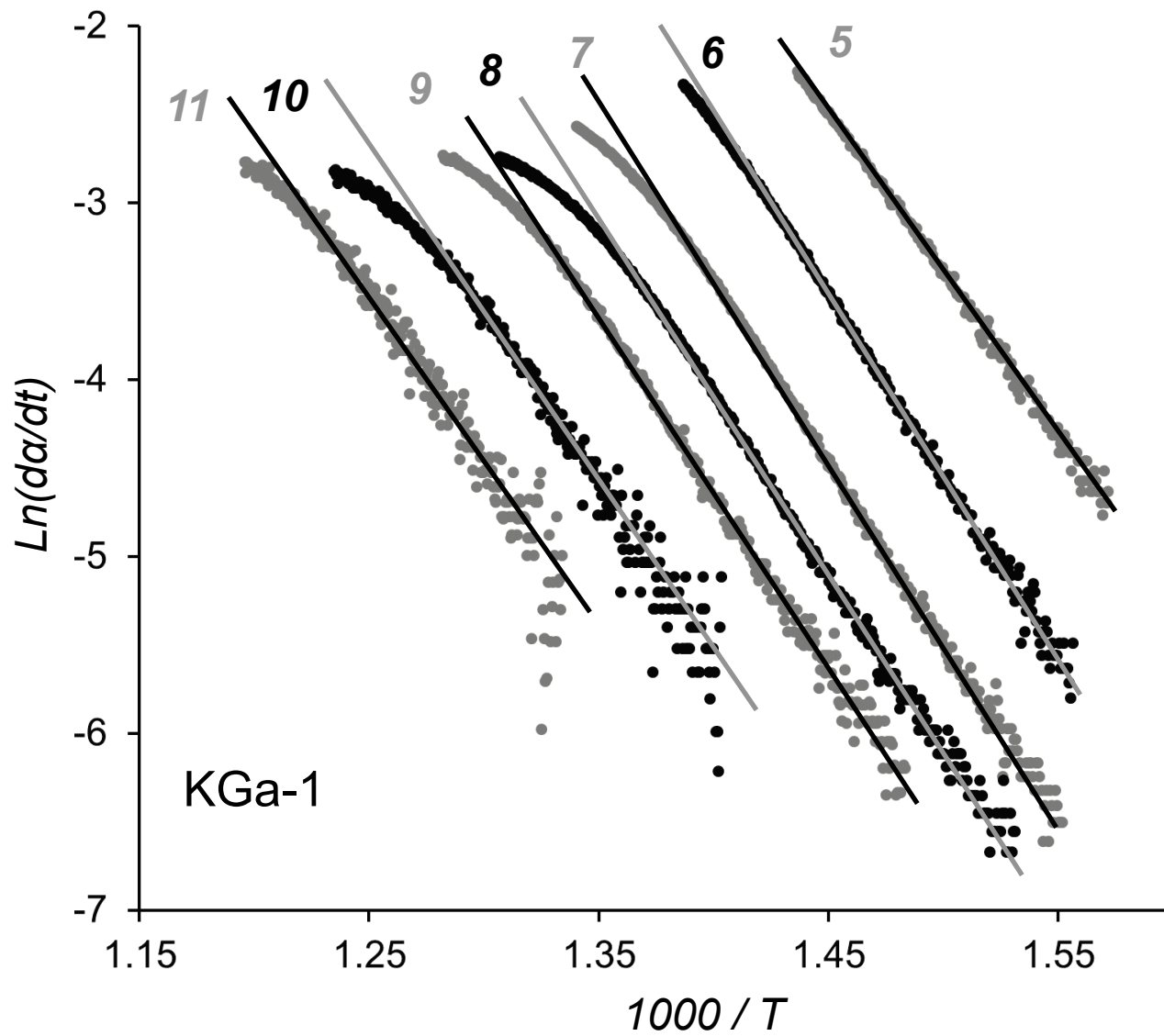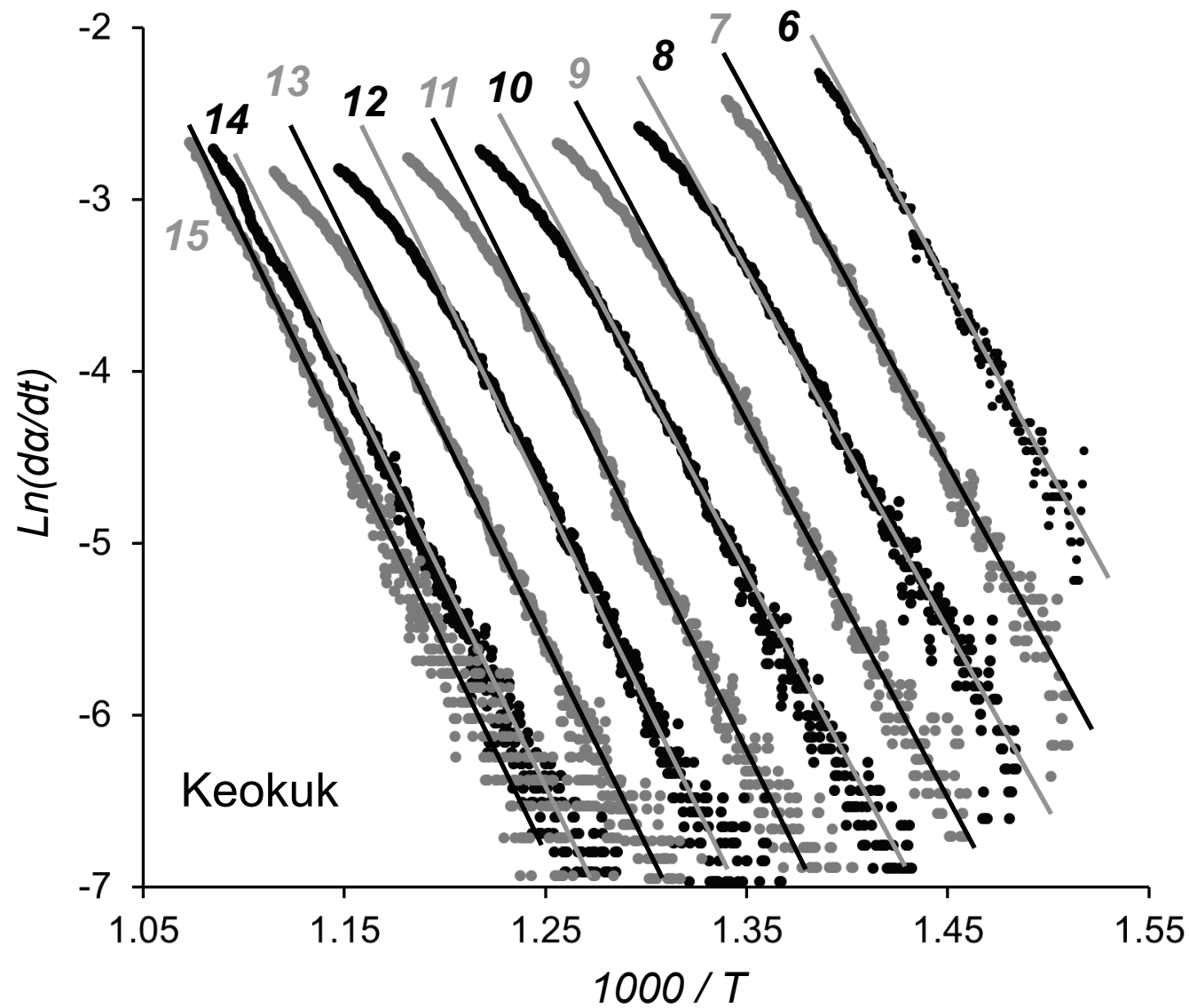
Figure 6 (panel 3)
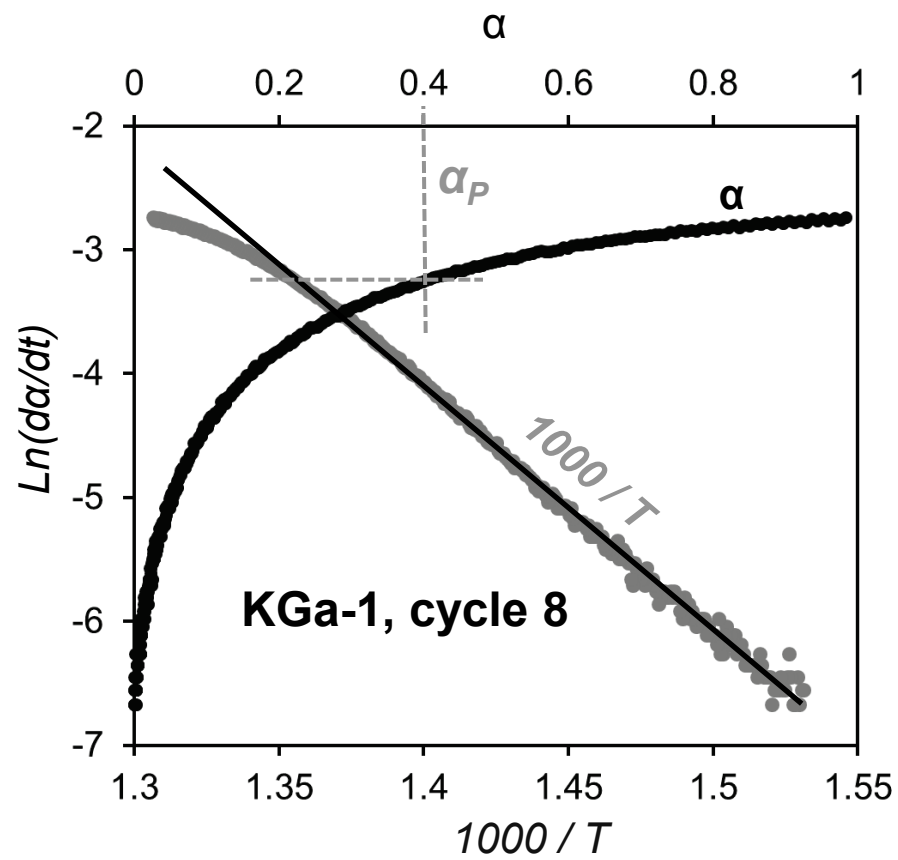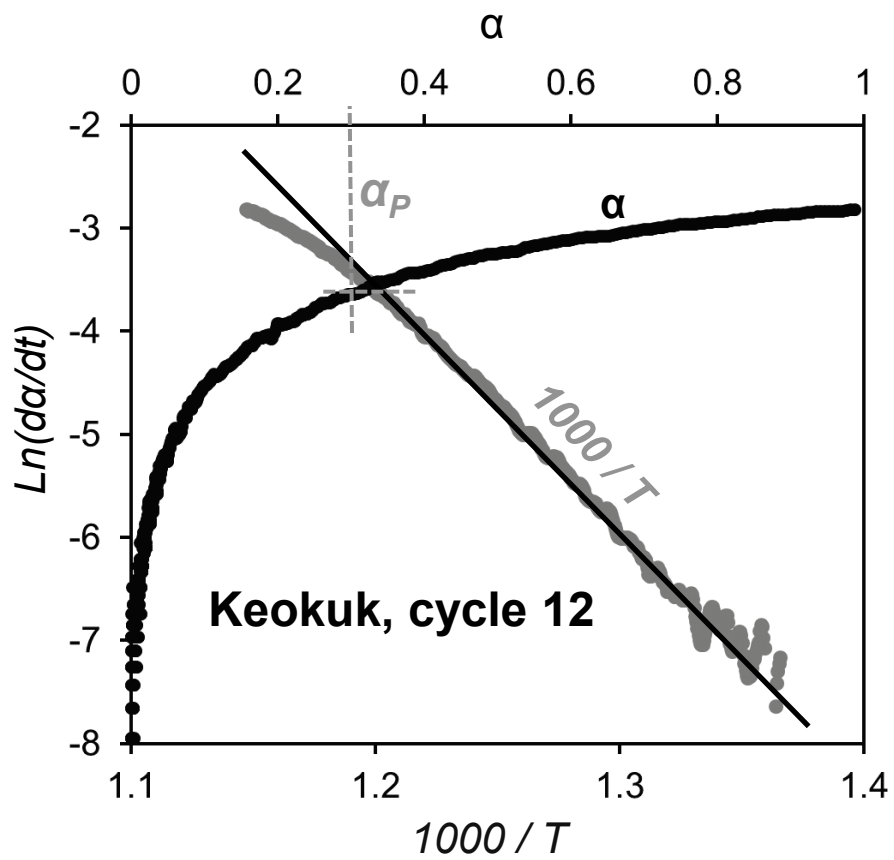
Figure 7
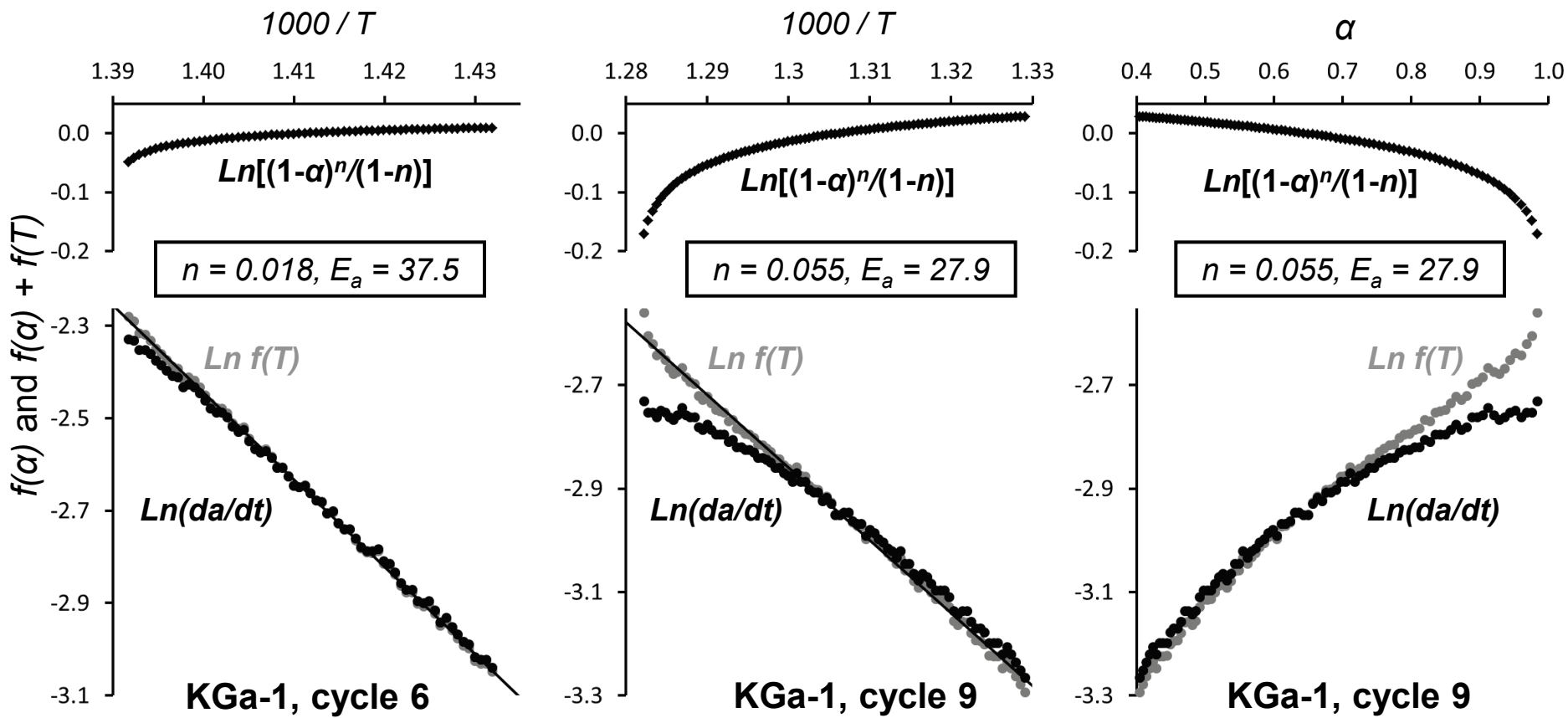
Figure 8
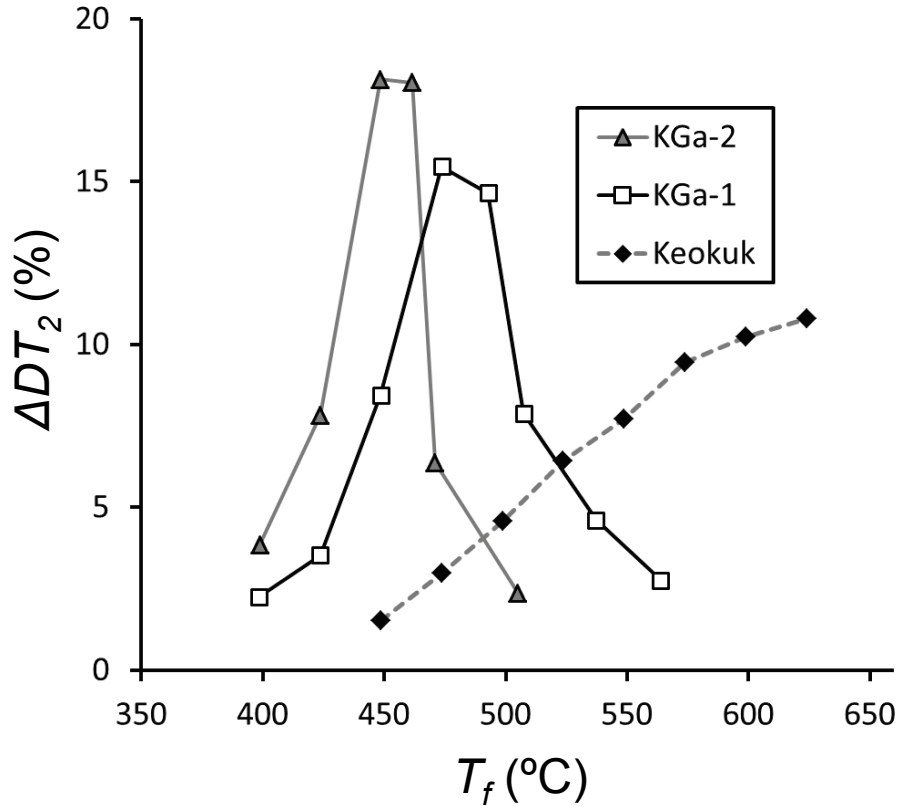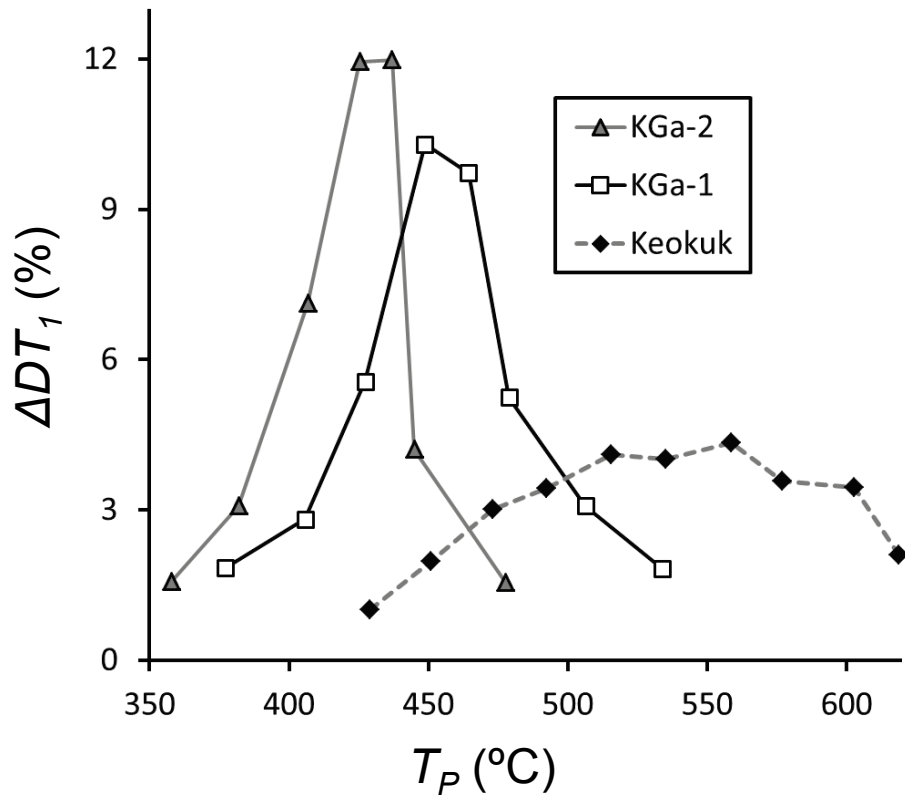
Figure 9
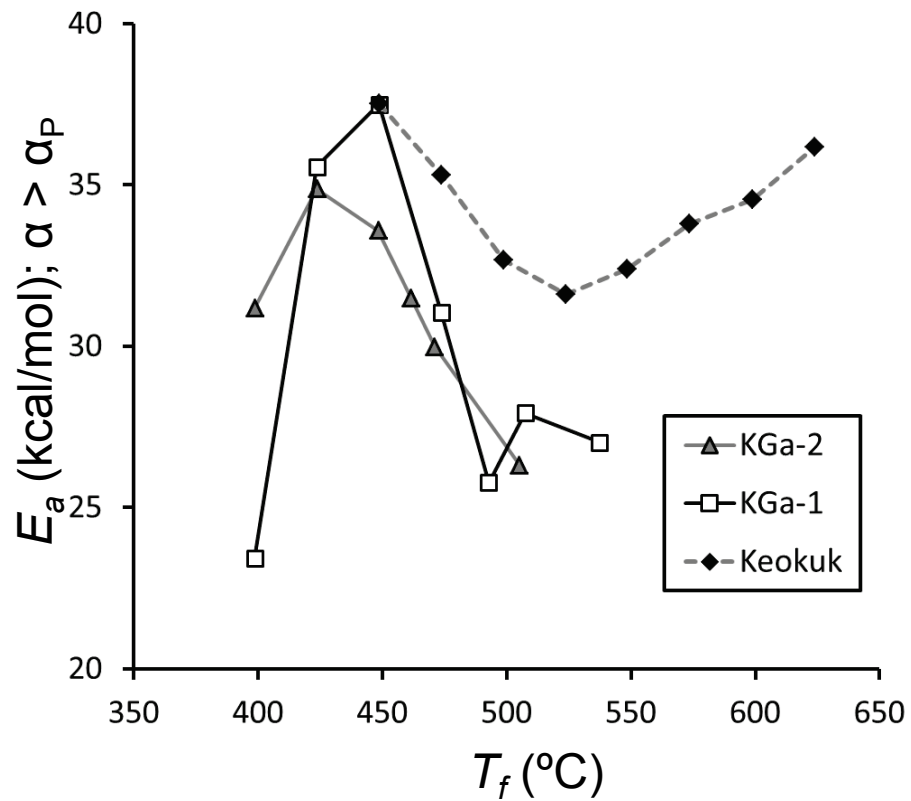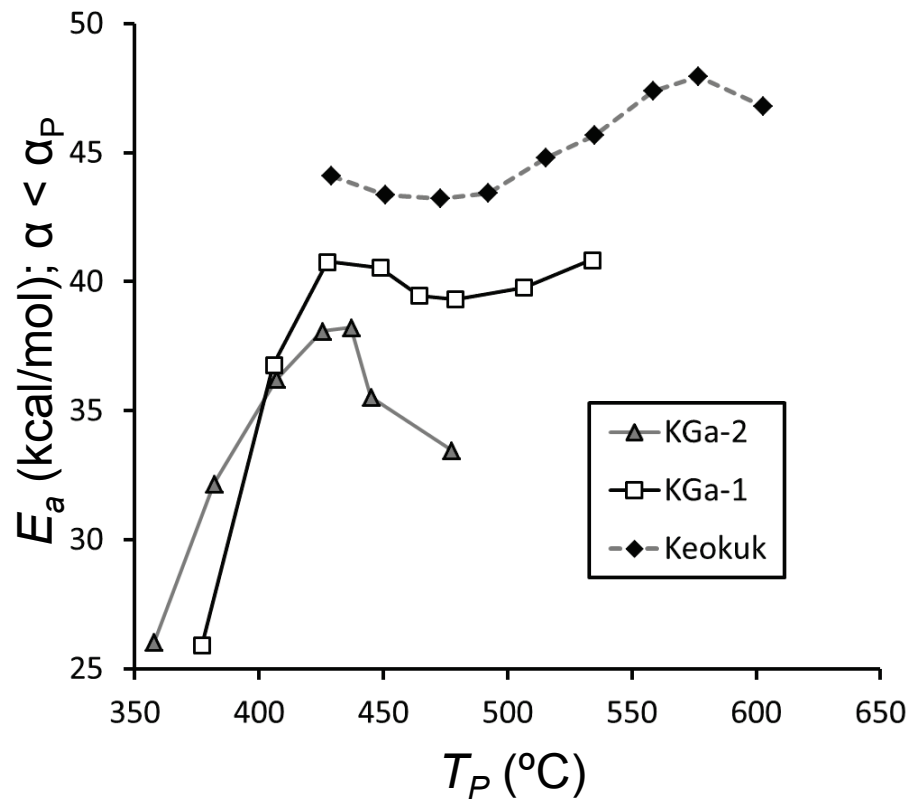
Figure 10
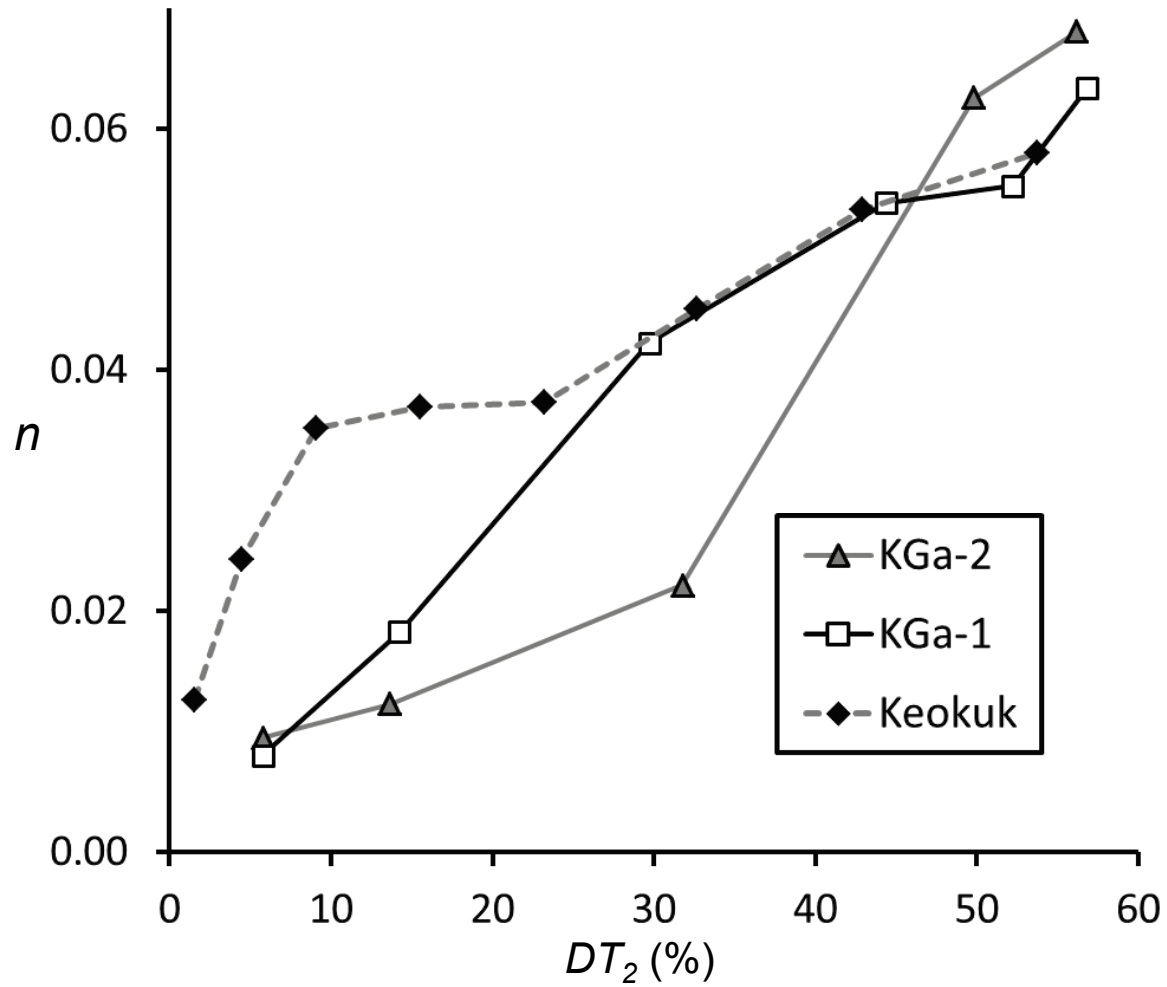
Figure 11
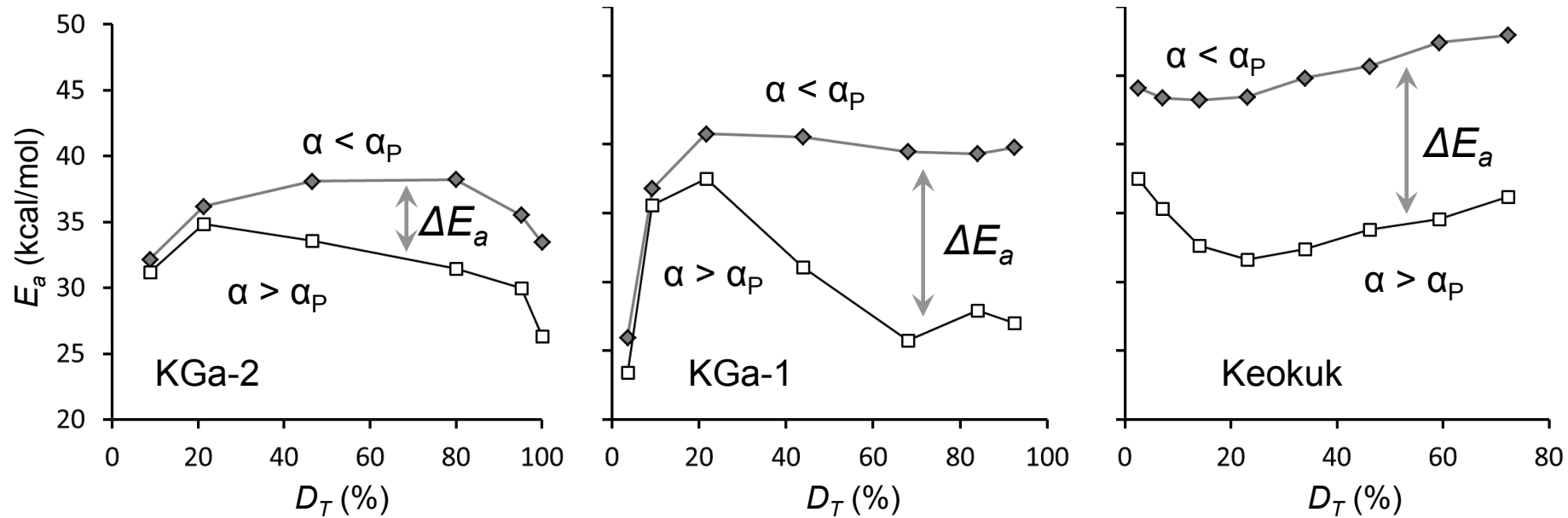
Figure 12
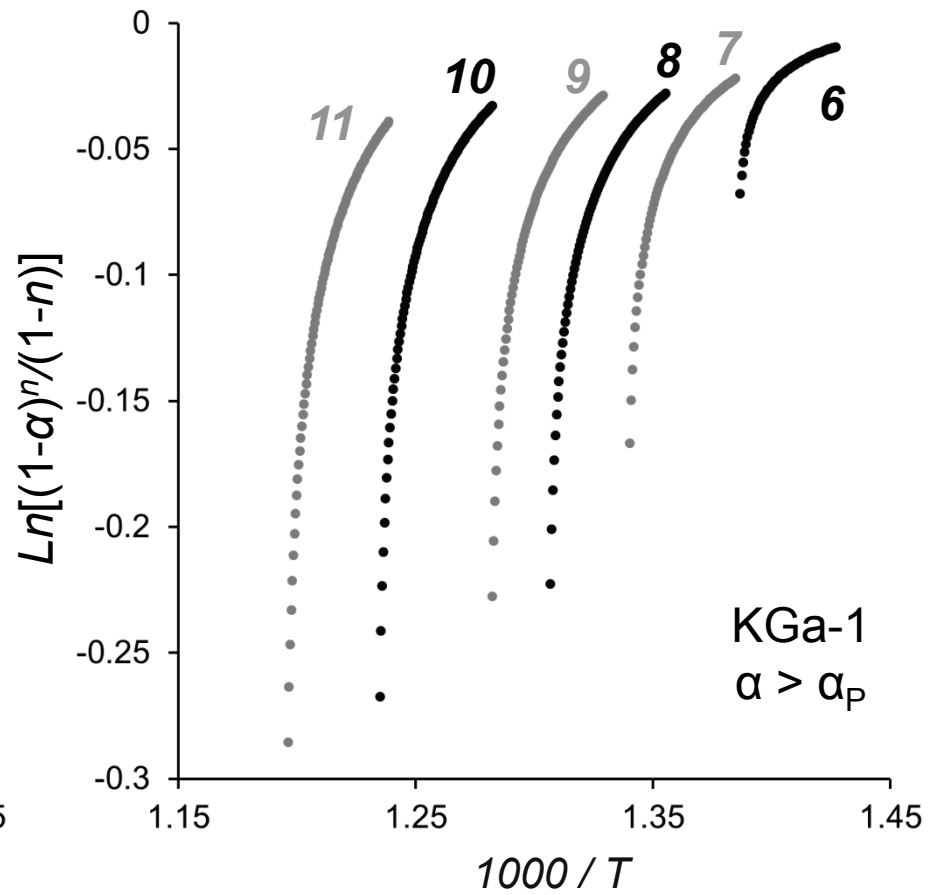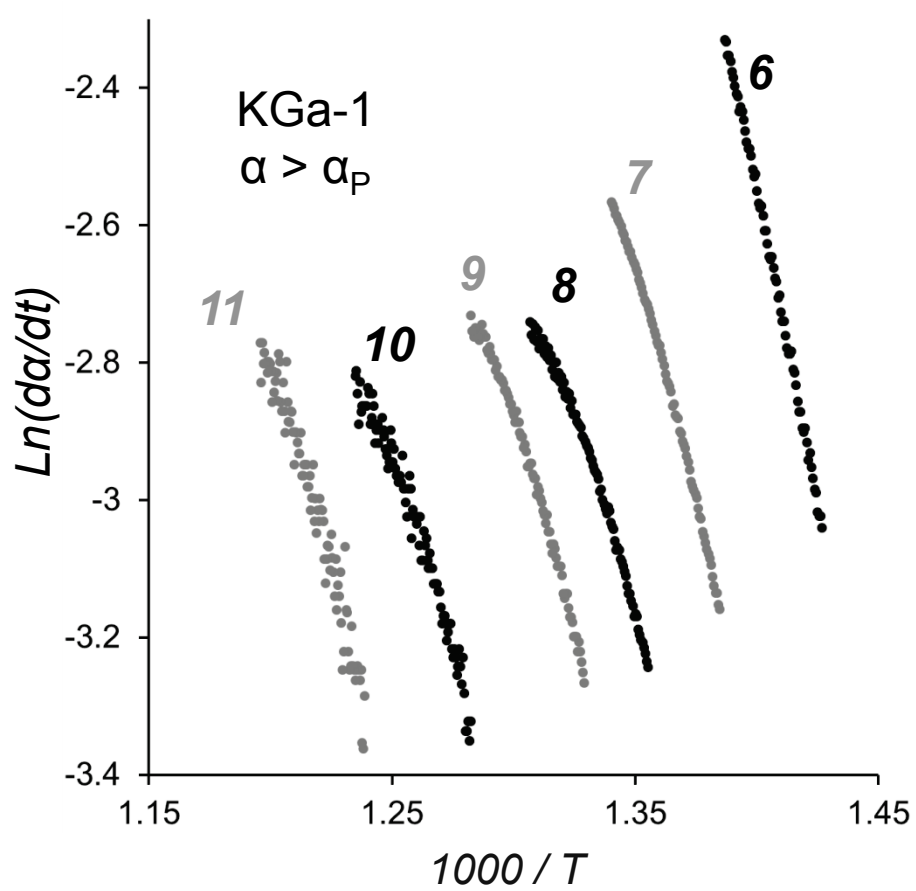
Figure 13

Table 1. Analytical results of the heating-cooling experiments and the calculations of kinetic parameters. For labels and abbreviations see the text.

Cycle No.	MCT (°C)	T_S (°C)	T_f (°C)	α_P	T_P (°C)	D_T (%)	ΔD_T (%)	DT_1 (%)	ΔDT_1 (%)	DT_2 (%)	ΔDT_2 (%)	For $\alpha < \alpha_P$ (Equation 7) E_a (kcal/mol)	r^2	For $\alpha > \alpha_P$ (Equation 8) E_a (kcal/mol)	r^2	n	ΔE_a (kcal/mol)
KGa-1																	
4	400	335	399	0.45	377	3.6	3.6	1.8	1.8	2.3	2.3	25.9	0.9618	23.4	0.9853	0.0042	2.5
5	425	363	424	0.45	406	9.3	5.6	4.7	2.8	5.8	3.5	36.8	0.9933	35.6	0.9974	0.0080	1.2
6	450	369	449	0.4	427	21.6	12.4	10.2	5.6	14.2	8.4	40.8	0.9955	37.5	0.9989	0.0182	3.3
7	475	371	474	0.4	449	43.9	22.3	20.5	10.3	29.7	15.5	40.5	0.9973	31.1	0.9984	0.0422	9.5
8	500	380	493	0.4	464	67.9	24.0	30.2	9.7	44.4	14.7	39.5	0.9971	25.8	0.9959	0.0539	13.7
9	525	401	507	0.4	479	84.0	16.0	35.5	5.2	52.2	7.9	39.3	0.9947	27.9	0.9967	0.0552	11.4
10	550	439	537	0.4	506	92.4	8.4	38.6	3.1	56.8	4.6	39.8	0.9690	27.0	0.9845	0.0634	12.8
11	575	476	564	0.4	534	100.0	7.6	40.4	1.8	59.6	2.8	40.8	0.9247	33.3	0.9769	0.0757	7.6
KGa-2																	
4	375	334	374	0.45	358	3.0	3.0	1.6	1.6	2.0	2.0	26.0	0.9699	25.4	0.9789	0.0000	
5	400	351	399	0.45	382	8.8	5.8	4.6	3.1	5.8	3.8	32.2	0.9926	31.2	0.9942	0.0094	1.0
6	425	360	424	0.45	407	21.3	12.5	11.8	7.1	13.6	7.8	36.2	0.9986	34.9	0.9985	0.0123	1.3
7	450	364	448	0.4	425	46.6	25.3	23.7	11.9	31.8	18.1	38.1	0.9988	33.6	0.9994	0.0221	4.5
8	475	366	462	0.4	437	80.0	33.4	35.7	12.0	49.8	18.0	38.2	0.9981	31.5	0.9977	0.0626	6.7

9	500	383	471	0.4	445	95.2	15.2	39.9	4.2	56.2	6.4	35.5	0.9887	30.0	0.9949	0.0681	5.5
10	525	434	505	0.4	478	100.0	4.8	41.5	1.6	58.5	2.4	33.5	0.9758	26.3	0.9851	0.0497	7.1
Keokuk																	
6	450	386	449	0.4	429	2.4	2.4	1.0	1.0	1.5	1.5	44.1	0.9694	37.5	0.9947	0.0126	6.6
7	475	389	474	0.4	451	7.1	4.6	3.0	2.0	4.5	3.0	43.4	0.9793	35.3	0.9939	0.0242	8.1
8	500	400	499	0.4	473	14.1	7.0	6.0	3.0	9.1	4.6	43.2	0.9791	32.7	0.9965	0.0351	10.5
9	525	412	524	0.35	492	23.1	9.0	9.4	3.4	15.5	6.4	43.4	0.9815	31.6	0.9971	0.0369	11.8
10	550	425	549	0.35	516	33.9	10.8	13.5	4.1	23.2	7.7	44.8	0.9892	32.4	0.9972	0.0373	12.4
11	575	439	574	0.30	535	46.2	12.3	17.5	4.0	32.7	9.5	45.7	0.9734	33.8	0.9972	0.0450	11.9
12	600	458	599	0.30	559	59.3	13.1	21.8	4.3	42.9	10.2	47.4	0.9726	34.5	0.9971	0.0533	12.9
13	625	475	624	0.25	577	72.3	13.0	25.4	3.6	53.7	10.8	47.9	0.9814	36.2	0.9966	0.0579	11.8
14	650	493	649	0.25	603	91.3	19.0	28.9	3.4	64.1	10.4	46.8	0.9760				
15	675	503	659	0.30	619	100.0	8.7	31.0	2.1	69.0	5.0	39.4	0.9128				